Kremer−Grest Models for Commodity Polymer Melts: Linking Theory, Experiment, and Simulation at the Kuhn Scale

Ralf Everaers, Hossein Ali Karimi-Varzaneh, Frank Fleck, Nils Hojdis, and Carsten Svaneborg*

ACCESS | Metrics & More | Article Recommendations

ABSTRACT: The Kremer−Grest (KG) polymer model is a standard model for studying generic polymer properties in molecular dynamics simulations. It owes its popularity to its simplicity and computational efficiency, rather than its ability to represent specific polymers species and conditions. Here we show that by tuning the chain stiffness it is possible to adapt the KG model to model melts of real polymers. In particular, we provide mapping relations from KG to SI units for a wide range of commodity polymers. The connection between the experimental and the KG melts is made at the Kuhn scale, i.e., at the crossover from the chemistry-specific small scale to the universal large scale behavior. We expect Kuhn scale-mapped KG models to faithfully represent universal properties dominated by the large scale conformational statistics and dynamics of flexible polymers. In particular, we observe very good agreement between entanglement moduli of our KG models and the experimental moduli of the target polymers.
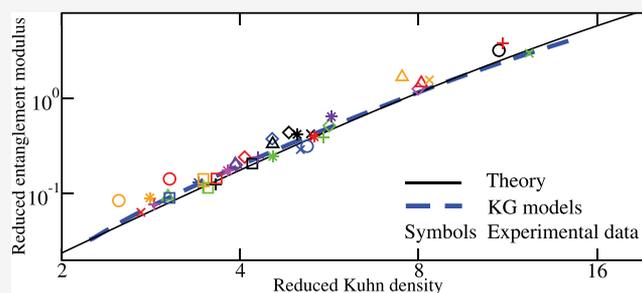
1. INTRODUCTION

Polymers are long chain molecules built by covalent linkage of a large numbers of identical monomers.[1,2] Synthetic polymers are ubiquitous in everyday life due to their unique processing and materials properties.[3] A key problem in polymer science is the relation between structure and dynamics on the molecular scale and the emergent macroscopic material properties. The bulk density, the temperature below which the materials become glassy,[4] or their ability to form semicrystalline phases[5] depends on specific chemical details at the monomer scale. Other properties, like the variation of the melt viscosity with the molecular weight of the chains, are controlled by the large scale conformational statistics and dynamics of long entangled chains, which adopt interpenetrating random walk conformations.[6] Such properties are characteristic of polymeric systems and universal[6,7] in the sense that a large number of chemically different systems exhibit identical behavior, if measurements are reported in suitable, material-specific units.

The character of the target properties is crucial for making an intelligent choice of which model to apply in a theoretical or computational investigation. Predicting specific material properties for a given chemical species often requires atom-scale modeling. A growing body of work aims at developing coarse-grained (CG) polymer models with lower resolution,[8−12] which are designed for specific polymer chemistries such as polyethylene,[13−15] polyisoprene,[16−19] polystyrene,[20−22] polyamide,[23,24] polymethacrylate,[25] polydimethylsiloxane,[19] bisphenol A polycarbonate,[26−28] polybutadiene,[29] vinyl polymers,[30] and polyisobutylene.[19] Common to these approaches

is the selected inclusion of specific chemical details in the coarse-grained models. They offer insights into which atomistic details of the chemical structure are relevant for particular nonuniversal polymer properties. The inclusion of molecular details is supposed to preserve a certain degree of transferability; i.e., models optimized to describe materials at one state point are expected to remain approximately valid at neighboring state points.[9,11,31] Similarly, careful coarse-graining is supposed to ensure representability, that is, the ability of a model to predict properties that it was not explicitly designed to reproduce.[32]

In contrast, universality is usually taken to justify a "one-model-fits-all" approach. For example, two polymer melts are expected to show identical rheological behavior, if the (linear) chains have the same *effective* length, Z in entanglement units, spatial distances in units of the tube diameter, d_T, and time in units of the entanglement time, τ_e. Here $Z = N/N_e$ where N denotes the chain length and N_e the chain length per entanglement. This suggests that the linear rheological behavior of a target material can be predicted on the basis of experimental reference data for particularly well-investigated

polymer species or by using simple, analytically[6,33−35] or numerically convenient lattice[36,37] and off-lattice models.[38,39]

A prototype example from polymer theory is the Rouse model of polymer dynamics,[40] which underlies the *phenomenological* tube model of entanglement effects in homopolymer melts.[6,33] Simulations targeting generic polymer behavior often employ the bead−spring polymer model introduced by Kremer and Grest (KG),[38,39] which is also central to the present work. In the KG model approximately hard-sphere beads are connected by strong nonlinear springs, generating the connectivity and the liquid-like monomer packing characteristic of polymer melts. The interactions are tuned to energetically prevent polymer chains from passing through each other. With the model reproducing the local topological constraints dominating the dynamics of long-chain polymers,[39] nontrivial large scale entanglement properties *emerge* through the exact same mechanisms as in real commodity polymer melts. While the parameters N_e, d_T, and τ_e characterizing the entanglement scale are direct input parameters of the tube model, they need to be *measured* as a function of the microscopic energy scale, ϵ, bead diameter, σ, mass, m_b, and time $\tau = \sigma\sqrt{m_b/\epsilon}$ of the KG model, before the simulation results can be related to experiment.[39]

Both the standard Rouse/tube and the KG model disregard the polymer contour length as an independent relevant length scale. Theorists assume Gaussian chain statistics, implicitly sending the contour length to infinity in the analytically convenient continuum limit. The contour length of KG chains is finite and well-defined, but because Kremer and Grest parametrized their model by mapping it to experimental systems on the entanglement scale, the value is essentially arbitrary. To describe situations where the chains undergo larger deformations, tube models incorporate their contour length as an additional, independent parameter.[6,33] But how should one control the chain length in KG-like models, where modifications of *microscopic* model parameters are bound to influence all emergent mesoscopic time and length scales?

At least qualitatively, finite extensibility was already accounted for in one of the oldest models of polymer physics. Kuhn's seminal insight in the 1930s was that the large scale conformations of chain molecules can be represented as an N_{eK} step random walk of "Kuhn" segments of length l_K.[41] For the proper choice of the Kuhn length, the model reproduces both the end-to-end distance at full extension, $L = l_K N_K$, and the mean-square end-to-end distance, $\langle R^2 \rangle = N_K l_K^2$, of target polymers. While the model obviously needs to be taken with a grain of salt, it provides polymer physics[6,7,42] with a natural set of microscopic units: the Kuhn length, l_K, the Kuhn time, τ_K, and $k_B T$ as the natural energy scale in entropy dominated systems. Intrinsically flexible polymers exhibit *universal* behavior[6,7,42] beyond the Kuhn scale, while behavior on smaller scales is material-specific and dependent on atomic details. For example, the large scale flexibility has completely different microscopic origins in the wormlike chain[43] and in the rotational-isomeric-state[2] models. Similarly, there are well-documented exceptions[44] to the strong form of the time−temperature superposition principle,[4] which postulates identical temperature dependence for microscopic relaxation mechanisms all the way down to the atomic scale. Work from the Hassager group[45] underlines the importance of the Kuhn scale for establishing universality in nonlinear rheology. In particular, the authors present three conditions for nonlinear

universality in the rheology of polymer melts.[45] In order for polymer melts to show identical behavior, they have (i) to be composed of chains with the same *effective* length, $Z = N_K/N_{eK}$, (ii) to have the same number of Kuhn segments per entanglement, N_{eK}, and (iii) to exhibit the same friction reduction in fast elongational flows.

Here we investigate how the KG model can be used as a convenient tool for exploring universal properties of *specific* polymer materials in the above, *extended* sense. This raises a number of questions: (1) Is there a minimal modification of the standard KG model that would allow for a coarse-grain description of the full range of standard commodity polymers? (2) How can KG models be related to atomistic simulations, which predict the emerging large scale behavior by accounting for chemical specificity on the atomic scale? (3) How can KG simulation results most easily be compared to theories of polymer physics? (4) How can KG simulations be used to predict the results of experiments performed on real polymers? (5) Is there a price to be paid in terms of computational efficiency in studying material-specific KG models compared to the standard use of the model?

The first question was addressed by Faller and Müller-Plathe,[46−48] who introduced a bending potential into the KG model. Here we show that by tuning the bending potential, we can reproduce the full range of effective stiffnesses exhibited by commodity polymers. In doing so, we rely on results of an accompanying paper, where we have studied the dependence of the characteristic time and length scales in KG bead−spring polymer melts on this parameter.[49] Our working hypothesis is that questions 2−4 can largely be reduced to a choice of units or the matching of key characteristic length and time scales. By construction, the resulting "Kuhn scale-mapped KG models" reproduce the ratio of the packing to Kuhn length of the target polymer. Interestingly, they turn out to be as or even more computationally efficient than the original model.

The paper is structured as follows. We review the necessary theoretical background in section 2. In section 2.1 we introduce with the Kuhn scale the units of length and time which are central to our scheme for locally mapping real polymers onto Kremer−Grest chains. The results cited in the remainder of section 2 serve to illustrate that two monodisperse polymer melts of chemically different polymers are expected to show the same universal large scale properties, provided (i) they are characterized by the same number of Kuhn segments per chain, N_K, (ii) their densities correspond to the same dimensionless Kuhn number, n_K, and (iii) properties are measured in the "natural" Kuhn units. The actual mapping is discussed in section 3. In section 3.2, we transcribe well-known results from Fetters et al.[50] for the chain structure of a wide range of commodity polymer melts to the Kuhn scale. Section 3.3 summarizes the results of the accompanying paper, where we have studied the dependence of the characteristic time and length scales in KG bead−spring polymer melts on the strength of the bending potential.[49] In section 3.4 we derive mapping relations for static properties. In particular, we provide tables specifying a one-parameter KG force field for a wide range of experimental polymer melts; that is, we list (1) which bending stiffness to use for modeling a particular chemical polymer species and (2) how to translate simulation results expressed in KG units into predictions for the specific polymer material expressed in SI units. Section 3.5 discusses the transferability of the force field to other temperatures. Section 3.6 focuses on time−temperature superposition as a

means of estimating of how simulation time in our KG models is related to real time. As a first test, we compare in section 3.7 plateau moduli inferred from KG models to experimental values. The discussion in section 4 focuses on the place of Kuhn scale matched KG models within the multiscale hierarchy of polymer polymers. We propose to view Kuhn scale matching as a special case of structure based coarse-graining and discuss the large effective time step of our models together with the expected speedup relative to atomistic simulations. Finally, we briefly conclude in section 5.

2. BACKGROUND

In this section, we provide a brief outline of polymer theory.[6,7,42,51] The point of the exercise is to show that Kuhn scale-mapped KG models can be expected to have predictive power for emergent polymer properties.

2.1. Kuhn Scale. The Kuhn length

$$l_K \stackrel{L \gg l_K}{=} \frac{\langle R^2 \rangle}{L} \tag{1}$$

characterizes the crossover from local rigid rod to random walk behavior. It is not straightforward to infer the Kuhn length from the chemical structure of a polymer in its melt state as it depends on intramolecular interactions, chemistry-specific local packing, and universal long-range correlations.[2,52,53]

A known Kuhn length can be used to characterize the large scale structure of polymer melts via two related dimensionless numbers. The number of Kuhn segments per chain

$$N_K = \frac{\langle R^2 \rangle}{l_K^2} = \frac{L^2}{\langle R^2 \rangle} \tag{2}$$

is a dimensionless measure of chain length. If ρ_K denotes the number density of Kuhn segments, then the number of Kuhn segments within the volume of a Kuhn length cube

$$n_K = \rho_K l_K^3 \tag{3}$$

provides a dimensionless measure of density for polymeric materials. We refer to n_K as the "Kuhn number". In Kuhn units, the chain density is given by

$$\rho_c = \frac{\rho_K}{N_K} \tag{4}$$

To characterize the dynamics, one can define the friction coefficient, ζ_K, of a Kuhn segment undergoing Brownian motion. Interpreting ζ_K as a viscous Stokes drag, $\zeta_K \propto \eta_K l_K$, it is convenient to define an effective viscosity at the Kuhn scale as

$$\eta_K = \frac{1}{36} \frac{\zeta_K}{l_K} \tag{5}$$

The fundamental time scale of the dynamics of intrinsically flexible polymers is set by the time that it takes a Kuhn segment to diffuse ($D_K = k_B T / \zeta_K$) over a distance comparable to its own size. Again, it turns out to be practical to incorporate some numerical prefactors into the definition of the Kuhn time:

$$\tau_K = \frac{1}{3\pi^2} \frac{\zeta_K l_K^2}{k_B T} = \frac{12}{\pi^2} \frac{\eta_K l_K^3}{k_B T} \tag{6}$$

The universal aspects of the mesoscale conformations[54,55] and liquid structure[56,57] *beyond* the Kuhn scale can often be

described by Gaussian chain models. This ansatz preserves the information about the mean-square chain extensions, $\langle R^2 \rangle$, without retaining the chain contour length, L, as relevant variable. This is particularly apparent in the continuum limit, which is frequently employed in theoretical calculations.[6,58]

2.2. Rouse Dynamics. We begin our short *tour d'horizon* with the Rouse model,[6,40] which describes the dynamics of short unentangled polymers. Rouse considered the Langevin dynamics of a "Gaussian" chain composed of beads, which experience local friction and which are connected by harmonic springs representing the entropic elasticity of polymer sections beyond the Kuhn scale. In this model, the maximal internal relaxation time of a chain is given by the Rouse time

$$\frac{\tau_R}{\tau_K} = N_K^2 \tag{7}$$

while the macroscopic melt viscosity can be written as

$$\frac{\eta}{\eta_K} = n_K N_K \tag{8}$$

In particular, eqs 7 and 8 illustrate the utility of the natural Kuhn units in expressing emergent universal properties.

2.3. Packing and the Invariant Degree of Polymerization. The key for understanding the properties of polymer melts is the realization that chains strongly interpenetrate. The Flory number

$$n_F = \rho_c \langle R^2 \rangle^{3/2} = n_K N_K^{1/2} \tag{9}$$

is defined as the number of chains populating, on average, the volume spanned by one chain. That the Flory number is large explains why chains behave nearly ideally in dense melts[59] and why such polymer systems can often be well described by mean-field theories.[60,61]

The invariant degree of polymerization

$$\bar{N} = \rho_c^2 \langle R^2 \rangle^3 = n_K^2 N_K = n_F^2 \tag{10}$$

is dimensionless measure of chain length *and* interpenetration and related to the number of intermolecular pair interactions a given reference chain experiences. It plays a key role in more complex polymer systems such as block copolymers undergoing micro phase separation.[55,62] The corresponding packing length[63,64] is defined as

$$p \equiv \sqrt{\frac{\langle R^2 \rangle}{\bar{N}}} = \frac{l_K}{n_K} = \frac{1}{\rho_c \langle R^2 \rangle} \tag{11}$$

such that monomers found at a spatial distance smaller than p from a reference monomer typically belong to the same chain. Monomers found at a larger distance have an increasing probability to belong to a different chain. It is evident from eq 10 that Kuhn matching is *sufficient* to reproduce *all* emergent properties in polymer melts, which depend of the invariant degree of polymerization, $\bar{N}$, but by no means *necessary*. For a more detailed discussion of these aspects in the context of multiscale modeling, we refer the reader to refs 65 and 66.

2.4. Entanglement Scale. Chains undergoing Brownian motion can slide past each other; however, their backbones cannot cross.[6] As a consequence, the motion of long chains is subject to long-lived topological constraints.[67] The constraints become relevant at scales beyond the entanglement (contour) length,[64,68] L_e, or the equivalent number of Kuhn units between entanglements, $N_{eK} = L_e/l_K$. In the present context N_{eK}

Table 1. Kuhn Descriptions and Entanglement Properties of Polymers[76] Characterized by Experimental Temperature T_{ref}, Mean-Square Extension per Molecular Mass $\langle R^2 \rangle / M_c$, Bulk Mass Density ρ_{bulk}, Entanglement Modulus G_e, and Derived Quantities Such As the Packing Length p and Tube Diameter d_T; Polymers Are Also Characterized by their Kuhn Number n_K, Kuhn Length l_K, Mass of a Kuhn Segment M_K, Kuhn Density ρ_K, the Reduced Entanglement Modulus $G_e l_K^3 / [k_B T_{\text{ref}}]$, Kuhn Segments between Entanglements N_{eK}, and Number of Entanglement Strands Per Entanglement Volume α^a

name	T_{ref} (K)	$\langle R^2 \rangle / M_c$ (Å²· mol/g)	ρ_{bulk} (g/ cm³)	G_e (MPa)	p (Å)	d_T (Å)	n_K	l_K (Å)	M_K (g/ mol)	M_K/ M_m	ρ_K (nm⁻³)	$G_e l_K^3/ k_B T$	N_{eK}	α
PI-50	298	0.528	0.893	0.51	3.52	47.7	2.50	8.80	146.60	2.15	3.66	0.085	29.41	13.6
PI-7	298	0.596	0.900	0.44	3.10	55.1	2.72	8.44	119.60	1.76	4.52	0.064	42.55	17.8
PDMS*	298	0.422	0.970	0.25	4.06	63.7	2.82	11.42	309.28	4.17	1.89	0.091	31.08	15.7
PI-20	298	0.591	0.898	0.44	3.13	54.8	2.86	8.98	136.50	2.00	3.95	0.077	37.17	17.5
PI-34	298	0.585	0.965	0.44	2.94	56.5	3.02	9.58	156.90	2.30	3.44	0.093	32.32	19.2
cis-PBd	298	0.758	0.900	0.95	2.43	42.2	3.40	8.28	90.50	1.67	5.99	0.131	25.93	17.3
PIB(413)	413	0.557	0.849	0.38	3.51	65.8	3.47	12.20	267.90	4.77	1.91	0.119	29.02	18.7
cis-PI	298	0.679	0.910	0.72	2.69	46.0	3.47	9.34	128.60	1.89	4.26	0.144	24.15	17.1
a-PP(463)	463	0.678	0.765	0.53	3.20	61.7	3.53	11.20	183.40	4.36	2.51	0.115	30.59	19.3
i-PP	463	0.694	0.766	0.54	3.12	61.7	3.64	11.40	187.80	4.46	2.46	0.125	29.22	19.8
a-PP(413)	413	0.678	0.791	0.59	3.10	56.0	3.65	11.20	183.40	4.36	2.60	0.145	25.21	18.1
a-PP(348)	348	0.678	0.825	0.60	2.97	51.9	3.81	11.20	183.40	4.36	2.71	0.175	21.70	17.5
a-PP	298	0.678	0.852	0.60	2.87	48.8	3.92	11.20	183.40	4.36	2.79	0.205	19.15	17.0
PIB	298	0.570	0.918	0.43	3.17	55.2	3.94	12.50	274.20	4.89	2.02	0.202	19.52	17.4
a-PMMA	413	0.390	1.130	0.39	3.77	62.5	4.07	15.30	598.00	5.97	1.14	0.243	16.72	16.6
i-PS*	413	0.420	0.969	0.24	4.08	76.7	4.19	17.11	697.12	6.69	0.84	0.209	20.10	18.8
a-PMA	298	0.436	1.110	0.31	3.43	61.9	4.29	14.70	494.60	5.75	1.35	0.241	17.79	18.1
PI-75	298	0.563	0.890	0.46	3.31	51.8	4.53	15.00	399.30	5.86	1.34	0.379	11.94	15.6
PBd-20	298	0.841	0.895	1.34	2.21	37.3	4.54	10.10	122.40	2.26	4.41	0.335	13.55	16.9
a-PS*	413	0.437	0.969	0.25	3.92	76.3	4.54	17.80	725.34	6.96	0.80	0.247	18.35	19.4
PBd-98	300	0.661	0.890	0.71	2.82	45.4	4.83	13.70	284.80	5.27	1.88	0.442	10.93	16.1
PEO*	353	0.805	1.060	2.25	1.95	33.4	4.99	9.71	117.12	2.66	5.45	0.423	11.81	17.1
POM*	473	0.763	1.140	2.12	1.91	40.1	5.06	9.65	122.11	4.07	5.62	0.293	17.28	21.0
a-PHMA	373	0.366	0.960	0.11	4.73	98.4	5.19	24.40	1622.00	9.53	0.36	0.317	16.35	20.8
a-PVA*	333	0.490	1.080	0.44	3.14	57.9	5.26	16.50	555.70	6.45	1.17	0.428	12.30	18.4
SBR	298	0.818	0.913	0.98	2.22	43.6	5.33	11.90	173.60	2.61	3.16	0.399	13.35	19.6
P6N*	543	0.853	0.985	2.25	1.98	41.1	5.53	10.93	140.05	1.24	4.24	0.392	14.11	20.8
a-PαMS*	473	0.442	1.040	0.40	3.61	67.2	5.66	20.43	944.61	7.99	0.66	0.523	10.82	18.6
a-PEA	298	0.463	1.130	0.45	3.17	53.7	5.70	18.10	710.10	7.09	0.96	0.649	8.79	16.9
PET*	548	0.845	0.989	3.88	1.99	31.3	7.50	14.91	263.15	1.37	2.26	1.698	4.42	15.8
s-PP	463	1.030	0.766	1.69	2.10	42.4	7.99	16.90	278.70	6.62	1.66	1.274	6.27	20.2
PE(413)	413	1.250	0.785	3.25	1.69	32.2	8.09	13.70	150.40	5.36	3.14	1.466	5.52	19.0
a-POA	298	0.442	0.980	0.20	3.83	73.3	8.34	31.90	2295.00	12.45	0.26	1.578	5.29	19.1
PC*	473	0.864	1.140	3.38	1.69	33.9	10.93	18.43	393.25	1.55	1.75	3.237	3.38	20.1
PE	298	1.400	0.851	4.38	1.39	26.0	11.10	15.40	168.30	6.00	3.04	3.884	2.86	18.6
PTFE*	653	0.598	1.460	2.12	1.90	47.2	12.30	23.40	915.41	9.15	0.96	3.019	4.07	24.8

^{a}The asterisk (∗) denotes polymers where we have derived the Kuhn scale descriptions; for the rest we use the values from ref [76] to uniquely identify polymers, and we have added the reference temperature to some of the polymer names.

> 1. The corresponding spatial scale is the so-called tube diameter

$$\frac{d_T}{l_K} = \sqrt{\frac{\langle R^2(N_{eK}) \rangle}{l_K^2}} = \sqrt{N_{eK}} \tag{12}$$

where the latter equality assumes $N_{eK} \gg 1$. Just like the fundamental time scale τ_K is determined by the Kuhn segment diffusion coefficient and the Kuhn length, the diffusion coefficient of an entanglement segment $(D_e = k_B T / [N_{eK} \zeta_K])$ and the tube diameter also define a characteristic time scale τ_e:

$$\frac{\tau_e}{\tau_K} = N_{eK}^2 \tag{13}$$

According to the packing argument for loosely entangled polymers,[69,70] the ratio of the tube diameter and the packing

length is given by a universal constant, α. Experimental results[50] (Table 1), simulation data,[49] and a geometric argument[71] for the local pairwise[72] entanglement of Gaussian chains suggest

$$\alpha = \frac{d_T}{p} = 18 \pm 2 \tag{14}$$

The packing argument implies that there are $\alpha = \frac{\rho_K}{N_{eK}} d_T^3$ entanglement strands per entanglement volume and that the entanglement length is given by

$$N_{eK} = \left(\frac{\alpha}{n_K} \right)^2 \tag{15}$$

Uchida et al.[73] developed a scaling theory to describe the crossover to the tightly entangled regime, suggesting instead

$$N_{eK} = x^{2/5}(1 + x^{2/5} + x^2)^{4/5} \quad \text{with } x = \frac{\alpha}{n_K} \tag{16}$$

For small Kuhn numbers, eq 16 agrees with the packing prediction, but corrections become noticeable for $n_K > 10$.

Above the entanglement time, the Rouse model fails to describe dynamic correlations in polymer melts. The universal behavior of entangled chains depends on chain length only through the number

$$Z = \frac{N_K}{N_{eK}} \tag{17}$$

of entanglements per chain and is best discussed in the "entanglement units" d_T and τ_e of spatial distance and time. A key point to note is that the simple relation $Z = \bar{N}/\alpha^2$ suggested by the packing argument breaks down when the Uchida corrections become relevant. In this case, the number of entanglements per chain, $Z(n_K)$, and the invariant index of polymerization, $\bar{N}(n_K)$, become *different* universal functions of the Kuhn number, n_K.

2.5. Tube Model. Modern theories of polymer dynamics[6] are based on the idea that entangled chains are confined to a one-dimensional, diffusive motion (reptation[74]) in tubelike regions in space.[75] In the limit of long chains the maximal relaxation time[74] is given by

$$\tau_{max} = 3Z^3\tau_e \tag{18}$$

and for $\tau_e < t < \tau_{max}$ the shear relaxation modulus, $G(t)$, exhibits a rubber-elastic plateau, $G_N = \frac{4}{5}G_e$, where the entanglement modulus

$$G_e = \frac{\rho_K}{N_{eK}}k_BT \tag{19}$$

is given by the product of entanglement density and thermal energy. From the time-dependent shear relaxation modulus one can obtain the shear compliance and the melt viscosity. The asymptotically expected result[6] for long entangled chains is given by

$$\eta = \frac{\pi^2}{15}G_e\tau_{max} \tag{20}$$

3. MATCHING AT THE KUHN SCALE

In section 2 we have identified three relevant length scales: the packing length, p, the Kuhn length, l_K, and the tube diameter, d_T. Polymer theory being typically directly formulated in terms of these scales, the results are straightforward to adjust to an experimental target system, for which p, l_K, and d_T are known. But in setting up computational models, we have to deal with the difficulty that the relevant polymer scales *emerge* from interactions and are only indirectly controlled through the parameters of the employed model. Does this mean that we need to embark on a complicated search for parameter combinations, which allow us to fulfill two independently controlled ratios like p/l_K and d_T/l_K? Or maybe one (the standard KG?) model "fits all", and it suffices to map its predictions to the various experimental target systems?

3.1. Case for Kuhn Scale Matching. As illustrated in section 2, *universal* static, dynamic, mesoscopic, and macroscopic properties of polymer melts emerge from the Kuhn scale. They depend on just two dimensionless parameters: the Kuhn number, n_K, characterizing the contour density of the

target material and the number of Kuhn segments per chain, N_K, as a measure of chain length(s). The first parameter is specific for the particular polymer chemistry, while the second characterizes the (polydisperse) composition of particular melts under investigation. Specifically, the matching of n_K assures that the model properly reproduces (i) the ratio of packing and Kuhn length, p/l_K (eq 11), (ii) the number of Kuhn segments per entanglement length, N_{eK} (eqs 15 and 16), (iii) the ratio of tube diameter and Kuhn length, d_T/l_K (eq 12), and (iv) the ratio of the Kuhn and entanglement times, τ_e/τ_K (eq 13). Matching N_K assures (i) comparable ratios of average and maximal chain elongation, $\langle R^2 \rangle/L^2 = 1/N_K$ (eq 1), (ii) comparable invariant degrees of polymerization, $\bar{N}$ (eq 10), (iii) comparable numbers of entanglements per chain, Z (eq 17), and (iv) comparable ratios of maximal relaxation and Kuhn time, τ_{max}/τ_K (eqs 7 and 18). Kuhn scale-mapped KG models can be expected to have predictive power for emergent polymer properties, if we may take it for granted that this universality of properties of different chemical species also extends to computational models that exhibit the key features of polymer melts: chain connectivity, local liquidlike monomer packing, and the impossibility of chain backbones to dynamically move through each other. To most convenient way to make predictions is (i) to express the simulation results for a suitable KG model in Kuhn units of the simulation model and (ii) to convert them to SI units by using the Kuhn length, l_K, Kuhn time, τ_K, Kuhn viscosity, η_K, and the thermal excitation energy, k_BT, for the specific target polymer.

3.2. Commodity Polymer Melts at the Kuhn Scale. At a given state point (temperature), a melt of monodisperse chains (with molecular weight M_c) can be characterized by just a few experimental observables: the mass density ρ_{bulk}, the average chain end-to-end distance per unit mass $\langle R^2 \rangle/M_c$, and the maximal chain extension, L. Values for these observables for a large number of typical polymers are collected in ref 76. We present data for a selected subset of polymers expressed in Kuhn units in Table 1. The Kuhn lengths are in the 1−2 nm range, with a Kuhn segment mass $M_K = M_c/N_K \sim 100$−2000 g/mol. The number of monomers in a Kuhn segment varies in the range 1−13, and the number density of Kuhn segments, ρ_K, varies in the range 0.5−5 nm^{-3}.

A key characteristic of polymer species is their Kuhn number, which varies for common, flexible commodity polymers in the range $2 \leq n_K \leq 12$. For comparison, $n_K > 10^4$ in gels of tightly entangled filamentous proteins such as F-actin.[77] In agreement with the arguments in the preceding section, we observe in Table 1 a systematic correlation between the Kuhn number and emergent properties such as the entanglement modulus and the entanglement length measured in Kuhn units. We will return to this point in section 3.7.

3.3. Kremer−Grest Model Polymer Melts at the Kuhn Scale. The Kremer−Grest model[38,39] is a de facto standard model in molecular dynamics investigations of generic polymer properties. The KG model is a bead−spring model, where the bead interact via a Lennard-Jones potential. Because we are not interested in studying the *emergence* of the glass transition,[78−80] we employ a version with purely repulsive Weeks−Chandler−Anderson (WCA) interactions (the 12−6 Lennard-Jones potential truncated and shifted to zero at the minimum)

$$U_{WCA}(r < 2^{1/6}\sigma) = 4k_BT\left[\left(\frac{\sigma}{r}\right)^{-12} - \left(\frac{\sigma}{r}\right)^{-6} + \frac{1}{4}\right] \quad (21)$$

where σ defines the bead diameter and where we have explicitly adopted the standard choice to render the model athermal by setting the energy scale of the WCA interaction equal to k_BT. Bonded beads interact through the finite-extensible-nonlinear spring (FENE) potential given by

$$U_{FENE}(r) = -15k_BT\left(\frac{R}{\sigma}\right)^2 \ln\left[1 - \left(\frac{r}{R}\right)^2\right] \quad (22)$$

We employ the standard choice of $R = 1.5\sigma$ for the distance, where the FENE potential diverges. The average bond length is $l_b = 0.965\sigma$. The standard choice for the bead density is $\rho_b = 0.85\sigma^{-3}$. Faller and Müller-Plathe[46−48] augmented the standard KG model with a bending potential

$$U_{bend}(\Theta) = \kappa\, k_BT(1 - \cos\Theta) \quad (23)$$

where Θ denotes the angle between subsequent bonds. To prepare this study, we have investigated the dependence of the characteristic time and length scales in KG bead−spring polymer melts on the reduced bending energy,.[49] In particular, we found for the Kuhn length

$$l_K(\kappa) = l_K^{(0)} + \Delta l_K$$

$$\frac{l_K^{(0)}(\kappa)}{\sigma} = \frac{l_b}{\sigma}\begin{cases} \dfrac{2\kappa + e^{-2\kappa} - 1}{1 - e^{-2\kappa}(2\kappa + 1)} & \text{if } \kappa \neq 0 \\[2mm] 1 & \text{if } \kappa = 0 \end{cases}$$

$$\frac{\Delta l_K(\kappa)}{\sigma} = 0.77(\tanh(-0.03\kappa^2 - 0.41\kappa + 0.16) + 1) \quad (24)$$

From this relation, we can directly infer the dimensionless Kuhn number, eq 3, characterizing KG melts:

$$n_K(\kappa) = \rho_b l_b l_K^2(\kappa) \quad (25)$$

Finally, the number of Kuhn segments between entanglements, the bead friction, the Kuhn friction, and the Kuhn time of the KG model are given by

$$N_{eK}(\kappa) = -0.84\kappa^4 + 3.14\kappa^3 + 3.69\kappa^2 - 30.1\kappa + 39.3 \quad (26)$$

$$\frac{\zeta_b(\kappa)}{m_b/\tau} \approx 24 + 21n_K^{-1}(\kappa) \quad (27)$$

$$\frac{\zeta_K(\kappa)}{m_b/\tau} \approx (25 + 22n_K^{-1}(\kappa))\frac{l_K(\kappa)}{\sigma} \quad (28)$$

$$\frac{\tau_K(\kappa)}{\tau} \approx (0.84 + 0.73n_K^{-1}(\kappa))\frac{l_K^3(\kappa)}{\sigma^3} \quad (29)$$

The parametrization of the Kuhn length we believe to be valid for arbitrary values for stiffness κ, while the other relations hold for bending rigidities in the interval $-1 < \kappa < 2.5$. A negative chain stiffness partly counteracts the stiffness induced by excluded volume interactions between next-nearest beads along a chain and hence makes the chain more flexible than the standard KG model. We estimate that the error on the two frictions and the Kuhn time is 20%.

3.4. One Parameter Kremer−Grest "Force Field" for Commodity Polymer Melts.

To define a KG force field for a polymeric material, we match the dimensionless Kuhn numbers n_K characterizing the experimental system and the model polymer melt. A priori, this requires the numerical inversion of the combination of eqs 24 and 25 to identify the corresponding reduced stiffness to use in the KG model. As shown in Figure 1, the approximate relation

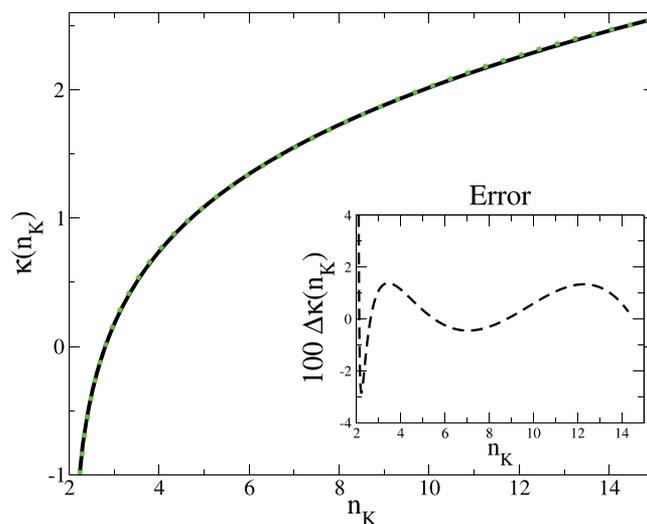$$\kappa(n_K) = 0.824\log(n_K - 2.0) - 0.00029n_K^3 + 0.0087n_K^2 - 0.055n_K + 0.28 \quad (30)$$

Figure 1. KG chain stiffness vs Kuhn number using eq 25 (solid black line) and our approximate inversion eq 30 (green symbols). The inset shows the error of our numerical inversion.

provides an excellent approximation over the experimentally relevant range $2 \leq n_K \leq 15$. Through eq 30, l_K, N_{eK}, ζ_K, and τ_K become functions of the Kuhn number. Note that the standard KG model with $\kappa = 0$ essentially corresponds to the intrinsically most flexible polymers such as PDMS or PI with 7−50% 3,4 content.

The number of beads per Kuhn length is given by

$$c_b(n_K) \equiv \frac{l_K}{l_b} = \sqrt{\frac{n_K}{\rho_b l_b^3}} \quad (31)$$

and hence the number of beads per chain required to model an experimental target polymer melt with chain length N_K is

$$N_b = c_b(n_K)N_K \quad (32)$$

What remains is to fix the mapping relations for the simulation units of length, mass, and time. Equating the model and experimental Kuhn lengths and accounting for the small difference, $l_b = 0.965\sigma$, between the bond length and the bead diameter in the KG model, we obtain

$$\sigma = \frac{l_K^{exp}}{0.965 \times c_b(n_K)} \quad (33)$$

The bead mass is obtained along the same lines by equating the experimental mass of a Kuhn segment to the mass of a Kuhn segment in the model:

Table 2. Kremer−Grest Model Parameters for the Polymers Shown in Table 1 in Terms of the Kuhn Number, Bending Stiffness κ, Number of Beads per Kuhn Segment c_b, Kuhn Length Expressed in KG units, Number of Beads per Monomer M_m/M_b, and Finally the Conversion Relations from KG Units for Energy $k_B T_{ref}$, Length σ, and Stress $k_B T_{ref} \sigma^{-3}$ to SI Units

name	n_K	κ	c_b	l_K/σ	M_m/M_b	M_b [g/mol]	$k_B T_{ref}$ (10^{-21} J)	σ (nm)	$k_B T_{ref} \sigma^{-3}$ (MPa)
PI-50	2.50	−0.378	1.81	1.74	0.84	81.13	4.11	0.50	32.0
PI-7	2.72	−0.086	1.89	1.82	1.07	63.37	4.11	0.46	41.3
PDMS*	2.82	0.013	1.92	1.85	0.46	161.05	4.11	0.62	17.6
PI-20	2.86	0.056	1.94	1.87	0.97	70.50	4.11	0.48	37.1
PI-34	3.02	0.191	1.99	1.92	0.86	78.86	4.11	0.50	33.1
cis-PBd	3.40	0.445	2.11	2.04	1.26	42.87	4.11	0.41	61.3
PIB(413)	3.47	0.483	2.13	2.06	0.45	125.69	5.70	0.59	27.3
cis-PI	3.47	0.484	2.13	2.06	1.13	60.32	4.11	0.45	44.0
a-PP(463)	3.53	0.518	2.15	2.07	0.49	85.25	6.39	0.54	40.7
i-PP	3.64	0.575	2.18	2.11	0.49	85.96	6.39	0.54	40.4
a-PP(413)	3.65	0.580	2.19	2.11	0.50	83.84	5.70	0.53	38.2
a-PP(348)	3.81	0.656	2.23	2.16	0.51	82.08	4.80	0.52	34.3
a-PP	3.92	0.708	2.27	2.19	0.52	80.84	4.11	0.51	30.7
PIB	3.94	0.714	2.27	2.19	0.47	120.66	4.11	0.57	22.2
a-PMMA	4.07	0.770	2.31	2.23	0.39	258.82	5.70	0.69	17.6
i-PS*	4.19	0.819	2.35	2.26	0.35	297.22	5.70	0.76	13.2
a-PMA	4.29	0.856	2.37	2.29	0.41	208.42	4.11	0.64	15.6
PI-75	4.53	0.941	2.44	2.35	0.42	163.78	4.11	0.64	15.9
PBd-20	4.54	0.944	2.44	2.35	1.08	50.16	4.11	0.43	52.2
a-PS*	4.54	0.944	2.44	2.35	0.35	297.19	5.70	0.76	13.2
PBd-98	4.83	1.039	2.52	2.43	0.48	113.08	4.14	0.56	23.1
PEO*	4.99	1.086	2.56	2.47	0.96	45.77	4.87	0.39	80.2
POM*	5.06	1.105	2.58	2.48	0.63	47.40	6.53	0.39	111.5
a-PHMA	5.19	1.143	2.61	2.52	0.27	621.59	5.15	0.97	5.7
a-PVA*	5.26	1.162	2.63	2.53	0.41	211.52	4.60	0.65	16.7
SBR	5.33	1.182	2.65	2.55	1.01	65.62	4.11	0.47	40.6
P6N*	5.53	1.234	2.69	2.60	2.18	51.98	7.50	0.42	100.9
a-PαMS*	5.66	1.265	2.72	2.63	0.34	346.66	6.53	0.78	13.9
a-PEA	5.70	1.276	2.74	2.64	0.39	259.56	4.11	0.69	12.8
PET*	7.50	1.646	3.14	3.03	2.29	83.82	7.57	0.49	63.4
s-PP	7.99	1.728	3.24	3.12	0.49	86.03	6.39	0.54	40.5
PE(413)	8.09	1.744	3.26	3.14	0.61	46.15	5.70	0.44	69.0
a-POA	8.34	1.785	3.31	3.19	0.27	693.22	4.11	1.00	4.1
PC*	10.93	2.136	3.79	3.65	2.45	103.76	6.53	0.50	51.0
PE	11.10	2.156	3.82	3.68	0.64	44.07	4.11	0.42	56.4
PTFE*	12.30	2.291	4.02	3.87	0.44	227.70	9.02	0.60	41.1

$$M_b = \frac{M_K^{exp}}{c_b(n_K)} \tag{34}$$

In Table 2 we have listed the resulting Kremer−Grest model parameters and mappings for the polymer species shown in Table 1. By construction, the number of beads per Kuhn length is an increasing function of n_K and varies between 1.7 and 3.9. With $-0.4 \leq \kappa \leq 2.3$ the required stiffness parameters falls into the validity range of our empirical relations for Kuhn length, entanglement length, and Kuhn friction. Bead diameters vary between 4 and 10 Å; the energy scale is given by the thermal energy at the experimental temperature and varies within a factor of 2. Nevertheless, the KG unit of stress, 4 MPa $< k_B T \sigma^{-3} <$ 112 MPa, exhibits a much larger spread. As a rule of thumb, beads correspond to monomers. But there are important variations. To cite some examples: PA and PDMS (polyisoprene and polydimethylsiloxane) are effectively the most flexible chains, which map fairly well on the standard KG model with $\kappa \equiv 0$. PI beads have a diameter of 5 Å and represent one monomer; PDMS beads have a diameter of 6 Å and represent two monomers. PS (polystyrene) beads

represent three monomers and have with 7.6 Å a correspondingly larger diameter. PE (polyethylene) is among the effectively stiffest chains, which four beads per Kuhn length and $\kappa \approx 2$. PE beads represent 1.5 monomers; with 4 Å they are relatively small. PC (polycarbonate) is comparable to PE in effective stiffness. With a diameter of 5 Å, PC beads are comparable to PI beads. However, in the case of PC 2.5 beads are required to represent the more complex monomers, which is remarkably similar to two bead/ellipsoid models per monomer used by Tschöp et al.[26]

Note that while we provide force fields for materials like polyethylene (PE), polyoxymethylene (POM), poly(ethylene terephthalate) (PET), poly(butylene terephthalate) (PBT), polytetrafluoroethylene (PTFE), or isotactic polypropylene (i-PP), they cannot be expected to reproduce the tendency to form semicrystalline ordering. Such KG models should thus be taken with a grain of salt or, maybe, as a reminder that there is more to polymers than universal properties. Nonetheless, we note that coarse-grain models have been used to study crystallization,[81] and recently specialized KG models were

Table 3. Parameters and Characteristic Times for Commodity Polymer Melts and the Corresponding KG Models[a]

name	T_g (K)	T_{ref}^{dyn} (K)	τ_e^{exp} (s)	n_K	N_{eK}	$\tau_K(T_{ref}^{dyn})$ (ns)	$\eta_K(T_{ref}^{dyn})$ (mPa·s)	$\tau(T_{ref}^{dyn})$ (ns)	$\sigma(M_b/k_B T_{ref}^{dyn})^{1/2}$ (ps)
PI-7	206	298	1.9×10^{-5}	2.72	41.76	10.90	61.32	1.6	2.33
PDMS	150	298	1.1×10^{-7}	2.82	38.74	0.073	0.17	0.01	5.00
cis-PBd	174	298	8.8×10^{-8}	3.40	26.76	0.12	0.73	0.01	1.71
cis-PI	206	298	6.7×10^{-5}	3.47	25.80	100.69	418	11	2.22
a-PP	262	348	1.9×10^{-6}	3.81	21.82	3.99	11.22	0.4	2.77
PIB	201	298	1.1×10^{-3}	3.94	20.58	2597	4499	240	3.98
a-PS	375	453	3.4×10^{-4}	4.54	16.18	1299	1184	100	6.75
PEO	210	348	1.5×10^{-8}	4.99	13.87	0.078	0.34	0.005	1.55

[a]The first set of numbers defines the experimental input: the experimental glass transition temperature and the dynamic reference temperature T_{ref}^{dyn} for the experimental entanglement time τ_e (and/or more suitable VF parameters). Using the static mapping and, in particular, the Kuhn number n_K, we can infer the number of Kuhn segments per entanglement length, N_{eK}, from eq 15 or more refined estimates.[49,73] The Kuhn time, $\tau_K(T_{ref}^{dyn})$, and the viscosity at the Kuhn scale, $\eta_K(T_{ref}^{dyn})$, follow from eqs 6 and 13; the characteristic time scale, $\tau(T_{ref}^{dyn})$, of the corresponding Kuhn mapped KG model is given by eq 6. For comparison, we also list the estimate for τ that results from the static mapping. Finally, we can use eqs 35 and 36 to estimate τ_K, η_K, and τ over the entire TTS validity range (Figure 2). References for experimental data: PI-7,[87,88] PDMS,[89] cis-PDb,[89] cis-PI,[89] cis-PI,[90] a-PP,[91] and PEO.[92]

developed and optimized[82,83] to study crystallization phenomena.

3.5. Temperature Dependence of the Parameters. *A priori*, the parameters listed in Table 2 are only valid at the indicated reference temperatures, where the chain dimensions were determined experimentally. To model polymer melts at different temperatures, we have, in principle, to account for changes in (i) the single chain statistics and (ii) the overall density. While it is straightforward to rationalize[84] a temperature-dependent Kuhn length, temperature variations in n_K due to density changes result in less intuitive shifts in bead diameters and weights with temperature. This is a consequence of our choice to preserve the "canonical" KG bead density of $\rho_b = 0.85\sigma^{-3}$.

In practice, the static melt properties are relatively insensitive to changes of temperature: the relative density expansion coefficient is $d \ln \rho_{bulk}/dT \approx -6 \times 10^{-4}$ K^{-1}, while typical thermal chain expansion coefficients $|d \ln \langle R^2 \rangle(T)/dT| < 10^{-3}$ K^{-1}.[76] Because $n_K(T) \sim \rho_{bulk}\langle R^2 \rangle^2$, we obtain $|d \ln n_K(T)/dT| < 3 \times 10^{-3}$ K^{-1}. In the one case where ref 76 provides data, atactic polypropylene, the 50% increase in temperature over the interval 298 K $\leq T \leq$ 463 K causes a slight increase in density while apparently leaving the chain dimensions unchanged. The corresponding reduction of the Kuhn number from $n_K = 3.92$ to $n_K = 3.43$ suggests that when one changes the bead weights from 81 to 85 g/mol, the bead diameters change from 5.1 to 5.4 Å, while the required reduction of the bending stiffness decreases the Kuhn length in LJ units from $l_K = 2.19\sigma$ to $l_K = 2.07\sigma$. Compared to the dynamic effects discussed in the following section, it thus seems safe to transfer the κ, M_b, and σ values listed in Table 2 to other temperatures. Compared to the standard "one-model-fits-all commodity polymer melts" approach discussed in the Introduction, we thus suggest the use of chemistry-specific athermal models over the entire (not extremely wide) experimentally relevant temperature range. While the use of *entropic* springs is standard in coarse-grain polymer models since the earliest theories of rubber elasticity,[85] an entropic wormlike bending rigidity like in eq 23 might appear unusual. An alternative could be KG models with freely rotating bonds along the lines of ref 86. However, within the present ansatz the resulting behavior is described by an athermal bending term. Obviously, the relations provided above can be used to obtain an improved parametrization, if there is information

available about the end-to-end distance and bulk density at the state point of interest.

3.6. Time Mapping. To reproduce not only static but also dynamic properties of target systems, we require input on their Kuhn time, τ_K, or their effective viscosity, η_K, at the Kuhn scale. Equating with τ_K or η_K of the Kuhn mapped KG model, we can directly infer the value of the KG time unit τ in SI units from eq 6, since the value of $\kappa(n_K)$ is known via eq 30 for the Kuhn number of the experimental system. However, to carry out this program, we needed to overcome two difficulties.

While conceptually useful, τ_K and η_K are not straightforward to observe directly. Typically, one can extrapolate down to the Kuhn scale within a model, if there is information about (emergent) macroscopic behavior or time scales at some dynamic reference temperature, T_{ref}^{dyn}. Examples of observables that are more easily accessible experimentally, and from which we can obtain a time mapping, are the viscosity of unentangled chains, $\eta = n_K N_K \eta_K$, the entanglement time, $\tau_e = N_{eK}^2 \tau_K$, the Rouse time, $\tau_R = N_K^2 \tau_K$, and the terminal relaxation time, τ_{max}. Experimentally, the Kuhn time or equivalently the Kuhn friction can be obtained from neutron spin echo data[93] by applying expressions from Rouse theory to analyze the monomeric dynamics below the entanglement time scale as in our analysis of simulation data.[49] The entanglement time, τ_e, can be measured by oscillatory rheological experiments, dielectric relaxation, and transverse relaxation NMR measurements (see e.g. refs 35 and 94−96). We note that published estimates might be obtained by fitting data to expressions, which define these times by using conventions for prefactors, which differ from those we have adopted here.

The second difficulty is the pronounced temperature dependence of the chain dynamics in polymer melts. Most commodity polymer melts become glassy below a temperature T_g in or slightly below the experimentally relevant temperature range. As a consequence, even a small change in temperature can have a significant impact on the dynamics. Experimentally, time−temperature superposition (TTS)[4] is used to explore polymer dynamics over a much wider range of frequencies than those directly accessible to a given measurement instrument. Here we use this approach to estimate the Kuhn time at the temperature of interest, T, given a Kuhn time measured at the reference temperature, T_{ref}^{dyn}:

$$\frac{\tau_K(T)}{\tau_K(T_{\text{ref}}^{\text{dyn}})} = a_T(T, T_{\text{ref}}^{\text{dyn}}) \tag{35}$$

As discussed in the Appendix, the shift factor can be written as

$$\ln a_T(T, T_{\text{ref}}^{\text{dyn}}) = -\frac{C_{VF}(T - T_{\text{ref}}^{\text{dyn}})}{(T_{\text{ref}}^{\text{dyn}} - T_V)(T - T_V)} \tag{36}$$

Equation 36 should be valid above the glass transition temperature in the temperature range $[T_g, T_g + 100\ \text{K}]$. Here we use a "universal" Vogel–Fulcher constant $C_{VF} = \ln(10) \times 17.44 \times 51.6\ \text{K} = 2072\ \text{K}$. Similarly, we set $T_V = T_g - 51.6\ \text{K}$ for the Vogel temperature, where viscosities and associated time scales formally diverge. More detailed information and specific tables with fitted VF (or WLF, see the Appendix) parameters can be found in ref 4.

The mapping relations for the temperature-dependent conversion of the KG time τ resulting from eq 6 are shown in Table 3 and illustrated in Figure 2. The converted values
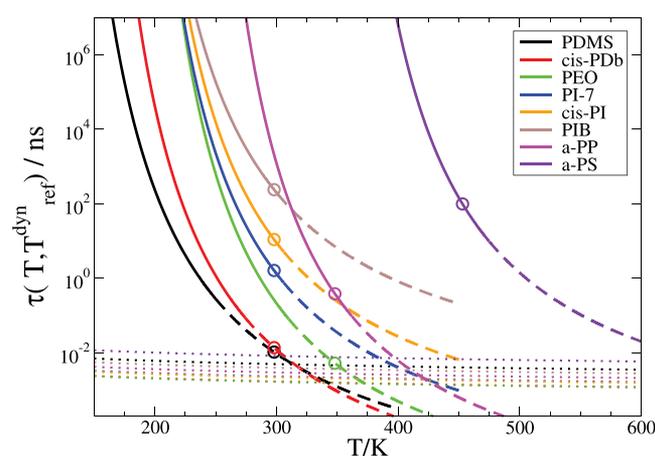
Figure 2. KG time unit τ (in ns) as a function of temperature for a number of polymer species listed in the legend and distinguished by color. Typical time steps in simulations are $\delta t = 10^{-2}\tau$. Solid lines: WLF extrapolation over the temperature range $[T_g, T_g + 100\ \text{K}]$. Thick dashed lines: WLF extrapolation for $T > T_g + 100\ \text{K}$. Symbols: estimate of τ derived from experimental data for the dynamic reference temperature, $T_{\text{ref}}^{\text{dyn}}$, underlying the WLF extrapolation. Thin dashed lines: standard estimation of the LJ time $\tau = \sigma\sqrt{M_b/[k_B T_{\text{ref}}^{\text{dyn}}]}$ using the mapping values for bead diameter, mass, and energy scale.

vary over a much wider range than the static parameters in Table 2: PDMS, cis-PDb, and PEO are experimentally studied about 150 K above T_g, resulting in KG time scales in the 10 ps range. PI melts at 100 K above T_g are represented by KG models with τ in the 10 ns range. PIB has a significantly higher $\tau \approx 240$ ns at a similar distance from the glass transition temperature. Perhaps this can be explained by specific intramolecular rotational barriers.[97] a-PS has a comparable $\tau \approx 100$ ns at 80 K above T_g, while a-PP maps onto a KG model with $\tau \approx 0.4$ ns at a comparable distance from T_g

3.7. First Test: Plateau Moduli of Commodity Polymer Melts. Figure 3 shows the reduced entanglement moduli as a function of Kuhn number. The experimental data are in good agreement with eq 19 for flexible chains.[50] The scatter observed between the experimental plateau moduli and the predicted plateau modulus line must be attributed either to chemical details causing some small degree of nonuniversal
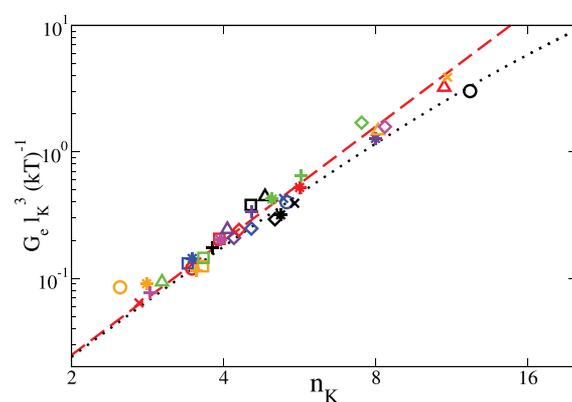

Figure 3. Reduced entanglement moduli for the polymers in Table 1 compared to the theoretical expectation for flexible polymers (eq 19) (red dashed line) to the semiempirical prediction of eq 42 in ref 49) (black dotted line). The symbols denote in order of increasing Kuhn number: PI-50 (orange ○), PI-7 (red ✕), PDMS (orange ∗), PI-20 (magenta +), PI-34 (green △), cis-PBd (blue □), PIB(413) (red ○), cis-PI (blue ∗), a-PP(463) (orange +), i-PP (orange □), a-PP(413) (green □), a-PP(348) (black +), a-PP (red □), PIB (magenta ∗), a-PMMA (indigo △), i-PS (indigo ◇), a-PMA (red ◇), PI-75 (black □), PBd-20 (indigo +), a-PS (blue ◇), PBd-98 (black △), PEO (green ∗), POM (black ◇), a-PHMA (black ∗), a-PVA (blue ✕), SBR (blue ○), P6N (black), a-PαMS (red ∗), a-PEA (green +), PET (green ◇), s-PP (indigo ∗), PE(413) (orange △), a-POA (magenta ◇), PC (red △), PE (orange ✕), and PTFE (black ○).

behavior,[98] such as a non-negligible crystalline fraction, or to experimental uncertainties in accurately estimating the plateau modulus.[99] For the very largest Kuhn numbers, the experimental data points can not discriminate between the packing argument and the predicted crossover to the tightly entangled regime.[49,77]

Figure 4 shows a comparison between experimental plateau moduli and entanglement moduli of KG melts extracted from
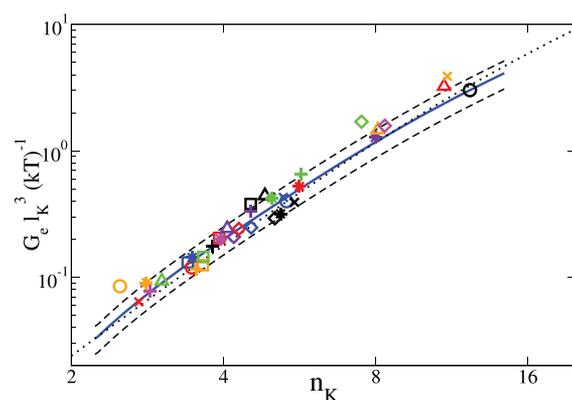

Figure 4. Reduced entanglement moduli for the experimental data in Figure 3 compared to the range of KG models for $-1 \leq \kappa \leq 2.5$ (blue solid line), with indications of $\pm 25\%$ error (dashed black lines). Also shown is the semiempirical prediction of eq 42 in ref 49) (black dotted line).

primitive path analysis.[49,100] Most of the experimental values are within the 25% error interval around the line defined by the one parameter KG models. This is concrete evidence that the emergent entanglement properties of our KG models agree with those of the targeted experimental polymer systems. Interestingly, the stiffer KG models also seem to be in excellent

agreement with the predicted crossover to tightly entangled regime.[49,77]

4. DISCUSSION

Polymeric systems exhibit a wide range of characteristic time and length scales. This is readily illustrated for the example of natural rubber, i.e. melts of cis-PI chains with a typical length of $N_K = 10^4$ Kuhn segments. Important characteristic length scales comprise (i) the Kuhn length, $l_K \approx 1$ nm, (ii) the tube diameter, $d_T \approx 5$ nm, (iii) the coil diameter, $\langle R^2 \rangle \approx 100$ nm, and (iv) the contour length, $L \approx 10$ μm. The spread is even larger between the characteristic time scales. There are already almost 3 orders of magnitude between the Kuhn time, $\tau_K \sim 1 \times 10^{-7}$ s, and the entanglement time, $\tau_e \sim 7 \times 10^{-5}$ s. The Rouse time of $\tau_R \sim 10^8 \tau_K \sim 10$ s governs *fast* processes such as the tension equilibration inside the tube,[6] while the estimated maximal relaxation time is $\tau_{\max} \sim 4$ h.

The slow dynamics has dramatic consequences for macroscopic properties such as the viscosity. Our estimate of the effective viscosity at the Kuhn scale is $\eta_K \approx 0.4$ Pa·s. The viscosity of a short chain melt at the entanglement threshold, $N_K = N_{eK}$, is already 2 orders of magnitude larger, $\eta_e \approx 40$ Pa·s, while for our strongly entangled ($Z = N_K/N_{eK} = 400$) example, $\eta \approx 5 \times 10^9$ Pa·s. In other words, the long chain melt exhibits a *macroscopic* viscosity similar to glass-forming liquids close to T_g, even though locally the chains experience a friction as if they were immersed in motor oil.

The wide range of relevant time and length scales in polymeric systems makes them natural targets for multiscale modeling.[11,101,102] In particle-based models, the resolution ranges from the atom scale to DPD-like descriptions, where entire chains are represented by one or two soft spheres or ellipsoids.[65,103] What is the natural place of KG-like models in this hierarchy? And how should they be parametrized?

4.1. Entanglement vs Kuhn Scale as Targets for KG Models. Typically, the KG model is mapped to experiments[34,39] or simulations of more microscopic models[105] on the entanglement scale. The mini-review in section 2.1 explains in some more detail the statement from the Introduction that one can hope to reproduce the large scale dynamics of a target system by carrying out KG simulation with chains of an appropriate effective length, $Z = L/L_e$, and then converting the results by identifying the tube diameter, d_T, as the unit of spatial distance as well as the entanglement time, τ_e, as the unit of time. Conceptually, this is what universality is all about and not different from using experimental data for PDMS to predict universal aspects of the behavior of, say, amorphous polystyrene.

Because in this view there is nothing special about the original KG model, one can apply the same logic to any other member of the family of KG models we are considering here. As illustrated by Figure 5, it is indeed tempting to use the additional stiffness parameter[47] to reduce the CPU time required to reach the entanglement scale.[48,106] But how far up the scales can one safely push the characteristic features of the KG model like the well-defined, almost inextensible contour length and the almost fully excluded molecular volume? These features are adequate for a description on the Kuhn scale but not for a generic model of loosely entangled chains at the entanglement scale.

Targeting the Kuhn scale, as we advocate here, provides a simple physical motivation for the choice of the stiffness parameter and should help to reduce "gaps"[105] relative to
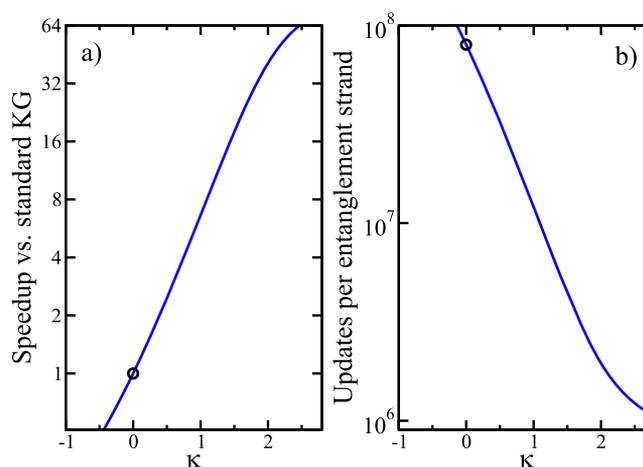

Figure 5. Speed-up of KG models due to increased stiffness. The left graph shows the speed up relative to the standard KG model with $\kappa = 0$, while the right graph shows the number of particle updates, $N_{eb} \frac{\tau_e}{\tau} \frac{\tau}{\delta}$, required to follow the dynamics of one entanglement strand over the entanglement time.

predictions of more microscopic models for the local behavior. Importantly, Kuhn scale-mapped KG models are in most cases computationally *more* efficient than the original KG model in reaching the entanglement scale, even though, by targeting the Kuhn scale, they are nominally more microscopic. The reason is that $\kappa > 0$ for most Kuhn scale-mapped KG models of commodity polymers, while the original KG model maps on the intrinsically most flexible polymer species. Typical speed-ups are of the order of 4; in the case of polycarbonate they reach a factor of 30 (Figure 5).

4.2. Linear vs Nonlinear Universality in the Rheology of Polymer Melts. Crucially, we can hope to extend the validity range of the KG model by, to paraphrase Einstein, making the chains "as stiff as possible, but not stiffer." By reproducing the number of Kuhn segments per entanglement length, N_{eK}, the models account for the maximal chain extension, $\sim \sqrt{N_{eK}}$, under strong deformations. Furthermore, KG melts parametrized at the Kuhn scale plausibly exhibit friction reduction in fast elongational flows, insofar as the effect can be attributed to the alignment of the Kuhn segments to the stretching direction.[107,108] There are thus good reasons to expect that the models discussed in the present article fulfill all three conditions for nonlinear universality in the rheology of polymer melts.[45]

4.3. Computational Performance of Kuhn Scale-Mapped KG Models Compared to Descriptions on Neighboring Scales. Kuhn scale-mapped KG models are computationally much less demanding than atomistic simulations. This is due to two factors: (i) There is a considerable reduction in the number of degrees of freedom. We have not counted atoms, but assuming carbon and hydrogen atoms as the dominant components, molecular bead weights between 40 and 700 g/mol translate to 3−50 united atoms that are being represented by one KG bead. If hydrogen atoms are represented explicitly, then these numbers increase by an additional factor of 2 or 3. (ii) At the reference temperature, $T_{\mathrm{ref}}^{\mathrm{dyn}}$, of the rheological experiments, our estimates for the physical meaning of the KG unit of time, τ, vary in the range 5 ps < 1τ < 0.24 μs. The corresponding time step of 50 fs < $\delta t = 10^{-2}\tau$ < 2.4 ns is thus 50 to 2.4 × 10^6 times larger than the

typical 1 fs time step in atomistic simulations. The time step in atomistic simulations is dictated by typical frequency of bond vibrations. Whereas if bond lengths are constrained, then the typical time scale is that of bond angle vibrations which occurs on time scales of tens of femtoseconds.[101,109] For systems closer to the glass transition, the speed-up in modeling the large scale behavior along the present lines would be exponentially larger. Compared to an atomistic model, this obviously comes at the price of loosing the ability to *predict* any of the glassy behavior.

With at least 10^6 particle updates per entanglement strand and time (inset of Figure 5), Kuhn scale-mapped KG models are bound to be slower than PPA-parametrized slip-link augmented DPD models.[110−114] Again, the more coarse-grain description benefits from a reduction of the number of degrees of freedom by a factor of the order of $1/N_{eK}$ as well as a corresponding reduction of the number of time steps by a factor of $\tau_K/\tau_e \sim 1/N_{eK}^2$. For the intrinsically most flexible polymers in Table 1, the speed-ups may be as large as a factor of 10^4 or even 10^5 in rare cases. While this approach is clearly successful, there is nevertheless a price to be paid: effects of topological constraints do not *emerge* through the same mechanisms as in the target systems. These effects have to be introduced explicitly in models developed at the entanglement scale. While the tube/slip-link model is in general well understood,[99] we suspect that nonlinear universality[45] or the emergence of crumpling in nonconcatenated ring melts[71,106] remains a challenge for such models.

4.4. Kuhn Scale Matching as a Special Case of Structure Based Coarse-Graining.
The construction of coarse-grain models requires choices and the definition of (subjective) priorities. A classic example is the tension between structure-based approaches[11,115,116] and schemes focused on preserving thermodynamic properties.[117]

Kuhn scale matching can be viewed as a special case of structure-based coarse-graining. It is guided by theoretical considerations which identify the Kuhn scale as controlling the emergent, universal behavior at larger time and length scales. Consequently, no particular effort is made to reproduce the local behavior. The resulting "one parameter force-field" for the KG model is remarkably simple, but this simplicity obviously comes at the price of losing the ability to predict (or to understand) the behavior of experimental target systems below the Kuhn scale. In particular, this holds on the bead scale, where we employ a computationally convenient, generic model without any particular relation to the properties (or the structure) of the target system.

The techniques for structure-based coarse-graining are well understood.[8,118−120] If applied on a similar level of coarse-graining as our KG models (i.e., retaining a comparable number of degrees of freedom), the resulting models can be expected to offer a locally more faithful representation. The differences are probably minor for polymers like isotactic polystyrene, where our KG beads represent three polystyrene monomers. The situation is different for polymers like polycarbonate, whose monomers are represented by several KG beads. In this case, the "beads" arising from systematic coarse-graining are neither of equal size, nor spherical, or nor joined in a straight line like those of our KG models.[8,26,103] Such models may provide insight into the relation between structure, local dynamics, and the dissipation mechanisms responsible for the glassy dynamics, which is lost in our approach. In terms of computational performance, they should

fall in between atomistic descriptions and Kuhn scale-mapped KG models, since they need to resolve motion on smaller time scales.

4.5. Time Scales in Coarse-Grain Models.
There is a persistent idea in the literature[34] that the time scale in simulations of coarse-grain models can be inferred by standard dimensional analysis. The difficulty becomes clear if we try to follow this approach on the Kuhn scale. The time scale $l_K\sqrt{M_K/k_\mathrm{B}T}$ can be understood as the time required by a Kuhn segment to ballistically cover a distance comparable to its size, l_K, if it moves at its thermal velocity, $v_K^\mathrm{th} = \sqrt{k_\mathrm{B}T/M_K}$. In contrast, the physically relevant Kuhn time, τ_K, is controlled by the local viscosity, eq 5, which emerges from microscopic interactions below the Kuhn scale and which is expected to display an exponential WLF temperature dependence (eqs 35 and 36).

The systematic linking of time scales on different levels of spatial and temporal resolution remains a challenge. A conceptual framework is provided by the Mori−Zwanzig projector formalism.[121,122] Here the projection operator is defined by the choice of "slow" CG variables. The formalism provides a generalized Langevin equation (GLE) for the time evolution of the CG variables, where the effect of the "fast" variables is described by the GLE memory kernel giving rise to friction and stochastic forces applied to the slow variables. In practice, sampling such GLE memory kernels requires simulations of the fast dynamics for fixed slow variables, which is complicated and has only been achieved relatively recently.[123−125]

In practice,[22] one often uses a mapping approach, where the time scale of the coarse-grain simulations is determined by the condition that the coarse-grain and the microscopic model predict identical dynamics on the largest time scales accessible to the microscopic approach. In the present case, we have used a mapping on the Kuhn scale to estimate the physical meaning of the KG time scale τ. As shown in Table 3 and Figure 2, these estimates exceed by orders of magnitude the time scale arising from the standard combination $\sigma\sqrt{M_b/[k_\mathrm{B}T_\mathrm{ref}^\mathrm{dyn}]}$ of the diameter and mass M_b of the KG beads with the energy scale of the model.

This mismatch strikes us as a natural and highly desired consequence of the elimination of microscopic degrees of freedom and of the associated dissipation mechanisms. In principle, it is possible to preserve $\sigma\sqrt{M_b/[k_\mathrm{B}T_\mathrm{ref}^\mathrm{dyn}]}$ as the definition of time by tuning the friction of a Langevin (or preferentially, DPD[126]) thermostat such that the resulting τ_K matches the experimental target value. However, this would make the simulations orders of magnitude more expensive in terms of computer time without providing additional physical insight.

4.6. Kuhn Scale Matched KG Models as Part of a Multiscale Hierarchy of Polymer Polymers.
In our opinion, the Kuhn scale merits to be systematically included in the hierarchy of multiscale models of polymeric systems. Omitting it risks to mask a remarkable simplicity, which emerges from the universality of polymeric behavior.

We have focused on the KG model with bending rigidity because it has been used in a vast number of publications as a basis for studying generic polymer and materials physics (see e.g. refs 11, 115, and 116 for reviews). Furthermore, there are several fast equilibration procedures[66,127,128] which allow to

build very well equilibrated, highly entangled melt configurations at relatively low computational cost. Obviously, one could apply the same logic to bead−spring models with variable density, to models based on chains of rods rather than beads,[129] or to lattice models[37,130−132] as long as these capture the relevant physics of polymers.

Kuhn scale-mapped polymer models are easy to connect to neighboring scales. In the "up" direction, the primitive path analysis[133] provides a systematic link to phenomenological models describing polymers on the entanglement scale.[110−114] For a comparison between the standard KG model and slip-link and slip-spring models see the recent work by Masubuchi and Uneyama.[104] In the "down" direction, they enable the generation of well-equilibrated atomistic material models through fine-graining of melt configurations of a chemistry-specific KG model.[134]

The information we used here to parametrize the KG model was obtained top-down from experiment.[76] Our aim was to provide reasonable estimates of these parameters for a wide variety of polymer species and over the entire experimentally relevant temperature range. Alternatively, one could analyze simulations of atomistic[13−19,25,29,30] or mildly coarse-grain[26−28] models of target polymers at specific state points. If the purpose is solely to parametrize the present model, then it suffices to analyze the simulations along the lines of the accompanying paper.[49] The inferred Kuhn length, density, and time are straightforward to convert into a bottom-up parametrization of the KG model, which then provides access to much larger time and length scales than the original, more microscopic model.

4.7. Possible Applications. Compared to the original KG model, the Kuhn scale-mapped variants are as or even more computationally efficient and can be expected to be predictive outside the linear regime. In particular, the mapping relations we provide should help to establish a direct, quantitative link to experiment. Otherwise, the models can be profitably applied to the same broad range of complex emergent phenomena as the original KG model. For instance, static and dynamic entanglement effects including multichain mechanisms such as constraint release[135−139] and crumpling[71,106,140,141] as well as correlation hole effects[53] will naturally emerge in such models, without the description needing to be accurate on the atomic scale. Polydispersity, branching,[142] chemical cross-linking,[143−145] and network aging[146] are also straightforward to include. Furthermore, such models can be used to study effects of spatial confinement[147] in thin films[148] and brushes,[149−151] or the addition of filler particles in composite materials,[152,153] or the welding dynamics at polymer interfaces,[154,155] to name a few examples.

5. CONCLUSION

We have argued that the Kuhn scale is a natural scale (i) to link theories, experiments, and simulations of amorphous polymer melts and (ii) to target in building computational polymer models. Omitting the Kuhn scale from the hierarchy of multiscale models risks to mask a remarkable simplicity, which emerges from the universality of polymeric behavior.

In practical terms, we have shown how to model homopolymer melts of a large variety of polymer species with an extension of the Kremer−Grest model,[38,39] which was originally introduced by Faller and Müller-Plathe.[46] The force field has a single adjustable parameter: the chain stiffness. We determine this parameter by matching the (Kuhn) number of

Kuhn segments per Kuhn volume, $n_K = \rho_K l_K^3$, of the target polymer species and the KG polymer model. No attempt is made to reproduce smaller scale features. Besides expressions for estimating the model parameters from experimental input, we have provided tables listing which bending stiffness to use for particular polymer species and how to translate KG into SI units. Our estimates for the mapping from simulation to physical time are based on time−temperature superposition.

Conceptually, Kuhn scale matching can be seen as a special case of structure based coarse-graining. The choice of the structural features to be preserved is guided by theoretical considerations, which identify the Kuhn scale as controlling the emergent universal polymer behavior at larger time and length scales.

The resulting coarse-graining level is about one bead per chemical monomer or two to three beads per Kuhn segment. Kuhn scale-mapped KG models thus fall in between atomistic or mildly coarse-grain models and descriptions on the entanglement scale. Both coarse-graining steps, from the atom to the Kuhn and from the Kuhn to the entanglement scale, are associated with performance gains of several orders of magnitude. For systems close to the glass transition, the speed-up in modeling the large scale behavior is even exponentially larger. Compared to atomistic descriptions, Kuhn scale-mapped KG models lose the ability to predict the microscopic (glassy) dynamics or to reproduce semicrystalline ordering. Compared to phenomenological entanglement models, Kuhn scale-mapped KG models preserve the emergence of the full spectrum of universal amorphous polymer properties through the same mechanisms as in the experimental target systems. In particular, we expect them to automatically fulfill all *three* conditions for nonlinear universality in the rheology of polymer melts.[45]

An interesting challenge for future work would be the parametrization of a corresponding force field for copolymer systems, using for example the technique from ref 156. While this should, in principle, be possible at least for static properties, modeling the dynamics might no longer be as simple as adjusting a single time scale. Similarly, it might be possible to parametrize minimal models of glassy[157,158] or semicrystalline[81] polymers along the present lines.

■ APPENDIX. TIME−TEMPERATURE SUPERPOSITION

For a TTS reference temperature T_0 the empirical Williams−Landel−Ferry (WLF)[159] shift factor has the form

$$\log a_T(T; T_0) = -\frac{C_1(T_0)(T - T_0)}{C_2(T_0) + (T - T_0)} \tag{37}$$

Equation 37 is valid above the glass transition temperature in the temperature range $[T_g, T_g + 100\ \text{K}]$. If one uses T_g as reference temperature, the constants adopt "universal" values $C_1^g \approx 15$ and $C_2^g \approx 50\ \text{K}$.[159] Other choices require suitably adjusted parameters $C_1(T_0)$ and $C_2(T_0)$.

The conversion can be avoided by writing the shift factor in a form derived from the equivalent Vogel−Fulcher−Tammann−Hesse equation.[160−162]

$$\ln a_T(T; T_0) = -\frac{C_{VF}(T - T_0)}{(T_0 - T_V)(T - T_V)} \tag{38}$$

The relations

$$T_V = T_0 - C_2(T_0) \Leftrightarrow C_2(T_0) = T_0 - T_V \qquad (39)$$

$$C_{VF} = \ln(10)C_1(T_0)C_2(T_0) \Leftrightarrow C_1(T_0) = \frac{C_{VF}}{\ln(10)(T_0 - T_V)} \qquad (40)$$

with $C_{VF} \approx 2000$ K allow to pass between the two representations. In particular, eqs 37 and 38 suggest (i) that the viscosity diverges at the Vogel temperature $T_V = T_g - C_2^g$ located ~ 50 K below the glass transition temperature and (ii) that the orders of magnitude by which the viscosity drops in the opposite limit of $T \to \infty$ are given by $C_1(T_0)$ and are hence inversely proportional to the distance of the reference from the Vogel temperature. More detailed information and specific tables can be found in ref 4. Note, however, that their eq 26.3 ought to read

$$\log a_T(T; T_0) = \frac{C_{VF}/\ln(10)}{T - T_V} - \frac{C_{VF}/\ln(10)}{T_0 - T_V} \qquad (41)$$

■ AUTHOR INFORMATION

Corresponding Author

Carsten Svaneborg − *University of Southern Denmark, DK-5230 Odense M, Denmark;* ● orcid.org/0000-0003-4301-3365; Email: science@zqex.dk

Authors

Ralf Everaers − *Université de Lyon, Ecole Normale Supérieure de Lyon, CNRS, Laboratoire de Physique and Centre Blaise Pascal de l'ENS de Lyon, F-69342 Lyon, France*

Hossein Ali Karimi-Varzaneh − *Continental Reifen Deutschland GmbH, D-30419 Hannover, Germany*

Frank Fleck − *Continental Reifen Deutschland GmbH, D-30419 Hannover, Germany*

Nils Hojdis − *Institute of Applied Polymer Chemistry, Aachen University of Applied Sciences, 52428 Jülich, Germany*

Complete contact information is available at:
https://pubs.acs.org/10.1021/acs.macromol.9b02428

Notes

The authors declare no competing financial interest.

■ ACKNOWLEDGMENTS

■ REFERENCES

(1) Flory, P. J. *Principles of Polymer Chemistry*; Cornell University Press: Ithaca, NY, 1953.

(2) Flory, P.; Volkenstein, M. *Statistical Mechanics of Chain Molecules*, 1969.

(3) McCrum, N. G.; Buckley, C.; Bucknall, C. B. *Principles of Polymer Engineering*; Oxford University Press: 1997.

(4) Ngai, K. L.; Plazek, D. J. *Physical Properties of Polymers Handbook*; Springer: 2007; p 455.

(5) Patlazhan, S.; Remond, Y. Structural mechanics of semicrystalline polymers prior to the yield point: A review. *J. Mater. Sci.* **2012**, *47*, 6749.

(6) Doi, M.; Edwards, S. F. *The Theory of Polymer Dynamics*; Clarendon: Oxford, 1986.

(7) de Gennes, P. G. *Scaling Concepts in Polymer Physics*; Cornell University Press: Ithaca, NY, 1979.

(8) Müller-Plathe, F. Coarse-graining in polymer simulation: From the atomistic to the mesoscopic scale and back. *ChemPhysChem* **2002**, *3*, 754.

(9) Baschnagel, J.; Binder, K.; Doruker, P.; Gusev, A. A.; Hahn, O.; Kremer, K.; Mattice, W. L.; Müller-Plathe, F.; Murat, M.; Paul, W. *Viscoelasticity, Atomistic Models, Statistical Chemistry*; Springer: 2000; p 41.

(10) Sun, Q.; Faller, R. Systematic coarse-graining of atomistic models for simulation of polymeric systems. *Comput. Chem. Eng.* **2005**, *29*, 2380.

(11) Peter, C.; Kremer, K. Multiscale simulation of soft matter systems - from the atomistic to the coarse-grained level and back. *Soft Matter* **2009**, *5*, 4357.

(12) Li, Y.; Abberton, B. C.; Kröger, M.; Liu, W. K. Challenges in multiscale modeling of polymer dynamics. *Polymers* **2013**, *5*, 751.

(13) Padding, J.; Briels, W. Time and length scales of polymer melts studied by coarse-grained Molecular Dynamics simulations. *J. Chem. Phys.* **2002**, *117*, 925.

(14) Liu, L.; Padding, J.; den Otter, W.; Briels, W. Coarse-grained simulations of moderately entangled star polyethylene melts. *J. Chem. Phys.* **2013**, *138*, 244912.

(15) Salerno, K. M.; Agrawal, A.; Perahia, D.; Grest, G. S. Resolving dynamic properties of polymers through coarse-grained computational studies. *Phys. Rev. Lett.* **2016**, *116*, No. 058302.

(16) Faller, R.; Müller-Plathe, F. Modeling of poly (isoprene) melts on different scales. *Polymer* **2002**, *43*, 621.

(17) Faller, R.; Reith, D. Properties of poly (isoprene): Model building in the melt and in solution. *Macromolecules* **2003**, *36*, 5406.

(18) Li, Y.; Kröger, M.; Liu, W. K. Primitive chain network study on uncrosslinked and crosslinked cis-polyisoprene polymers. *Polymer* **2011**, *52*, 5867.

(19) Maurel, G.; Goujon, F.; Schnell, B.; Malfreyt, P. Prediction of structural and thermomechanical properties of polymers from multiscale simulations. *RSC Adv.* **2015**, *5*, 14065.

(20) Harmandaris, V.; Adhikari, N.; van der Vegt, N. F.; Kremer, K. Hierarchical modeling of polystyrene: From atomistic to coarse-grained simulations. *Macromolecules* **2006**, *39*, 6708.

(21) Chen, X.; Carbone, P.; Cavalcanti, W. L.; Milano, G.; Müller-Plathe, F. Viscosity and structural alteration of a coarse-grained model of polystyrene under steady shear flow studied by reverse non-equilibrium Molecular Dynamics. *Macromolecules* **2007**, *40*, 8087.

(22) Fritz, D.; Koschke, K.; Harmandaris, V. A.; van der Vegt, N. F.; Kremer, K. Multiscale modeling of soft matter: Scaling of dynamics. *Phys. Chem. Chem. Phys.* **2011**, *13*, 10412.

(23) Karimi-Varzaneh, H. A.; Carbone, P.; Müller-Plathe, F. Fast dynamics in coarse-grained polymer models: The effect of the hydrogen bonds. *J. Chem. Phys.* **2008**, *129*, 154904.

(24) Eslami, H.; Karimi-Varzaneh, H. A.; Müller-Plathe, F. Coarse-grained computer simulation of nanoconfined polyamide-6, 6. *Macromolecules* **2011**, *44*, 3117.

(25) Chen, C.; Depa, P.; Maranas, J. K.; Sakai, V. G. Comparison of explicit atom, united atom, and coarse-grained simulations of poly (methyl methacrylate). *J. Chem. Phys.* **2008**, *128*, 124906.

(26) Tschöp, W.; Kremer, K.; Batoulis, J.; Bürger, T.; Hahn, O. Simulation of polymer melts. I. Coarse-graining procedure for polycarbonates. *Acta Polym.* **1998**, *49*, 61.

(27) Abrams, C. F.; Kremer, K. Combined coarse-grained and atomistic simulation of liquid bisphenol A-polycarbonate: Liquid packing and intramolecular structure. *Macromolecules* **2003**, *36*, 260.

(28) Hess, B.; León, S.; Van Der Vegt, N.; Kremer, K. Long time atomistic polymer trajectories from coarse grained simulations: bisphenol-A polycarbonate. *Soft Matter* **2006**, *2*, 409.

(29) Strauch, T.; Yelash, L.; Paul, W. A coarse-graining procedure for polymer melts applied to 1, 4-polybutadiene. *Phys. Chem. Chem. Phys.* **2009**, *11*, 1942.

(30) Milano, G.; Müller-Plathe, F. Mapping atomistic simulations to mesoscopic models: A systematic coarse-graining procedure for vinyl polymer chains. *J. Phys. Chem. B* **2005**, *109*, 18609.

(31) Carbone, P.; Varzaneh, H. A. K.; Chen, X.; Müller-Plathe, F. Transferability of coarse-grained force fields: The polymer case. *J. Chem. Phys.* **2008**, *128*, 064904.

(32) Johnson, M. E.; Head-Gordon, T.; Louis, A. A. Representability problems for coarse-grained water potentials. *J. Chem. Phys.* **2007**, *126*, 144509.

(33) Likhtman, A. E.; McLeish, T. C. Quantitative theory for linear dynamics of linear entangled polymers. *Macromolecules* **2002**, *35*, 6332.

(34) Kröger, M. Simple models for complex nonequilibrium fluids. *Phys. Rep.* **2004**, *390*, 453.

(35) McLeish, T. C. B. Tube theory of entangled polymer dynamics. *Adv. Phys.* **2002**, *51*, 1379.

(36) Binder, K. *Monte Carlo and Molecular Dynamics Simulations in Polymer Science*; Oxford University Press: New York, 1995.

(37) Carmesin, I.; Kremer, K. The bond fluctuation method: a new effective algorithm for the dynamics of polymers in all spatial dimensions. *Macromolecules* **1988**, *21*, 2819.

(38) Grest, G. S.; Kremer, K. Molecular Dynamics simulation for polymers in the presence of a heat bath. *Phys. Rev. A* **1986**, *33*, 3628.

(39) Kremer, K.; Grest, G. S. Dynamics of entangled linear polymer melts: A Molecular-Dynamics simulation. *J. Chem. Phys.* **1990**, *92*, 5057.

(40) Rouse, P. E. A theory of the linear viscoelastic properties of dilute solutions of coiling polymers. *J. Chem. Phys.* **1953**, *21*, 1272.

(41) Kuhn, W. Über die Gestalt fadenförmiger Moleküle in Lösung. *Colloid Polym. Sci.* **1934**, *68*, 2.

(42) Rubinstein, M.; Colby, R. H. *Polymer Physics*; Oxford University Press: New York, 2003.

(43) Kratky, O.; Porod, G. Röntgenuntersuchung gelöster Fadenmoleküle. *Rec. Trav. Chim.* **1949**, *68*, 1106.

(44) Ding, Y.; Sokolov, A. P. Breakdown of time-temperature superposition principle and universality of chain dynamics in polymers. *Macromolecules* **2006**, *39*, 3322.

(45) Wingstrand, S. L.; Alvarez, N. J.; Huang, Q.; Hassager, O. Linear and nonlinear universality in the rheology of polymer melts and solutions. *Phys. Rev. Lett.* **2015**, *115*, No. 078302.

(46) Faller, R.; Kolb, A.; Müller-Plathe, F. Local chain ordering in amorphous polymer melts: Influence of chain stiffness. *Phys. Chem. Chem. Phys.* **1999**, *1*, 2071.

(47) Faller, R.; Müller-Plathe, F.; Heuer, A. Local reorientation dynamics of semiflexible polymers in the melt. *Macromolecules* **2000**, *33*, 6602.

(48) Faller, R.; Müller-Plathe, F. Chain stiffness intensifies the reptation characteristics of polymer dynamics in the melt. *ChemPhysChem* **2001**, *2*, 180.

(49) Svaneborg, C.; Everaers, R. Characteristic time and length scales in Kremer-Grest bead-spring polymers with wormlike bending stiffness. *Macromolecules* **2020**, DOI: 10.1021/acs.macromol.9b02437.

(50) Fetters, L. J.; Lohse, D. J.; Richter, D.; Witten, T. A.; Zirkel, A. Connection between polymer molecular weight, density, chain dimensions, and melt viscoelastic properties. *Macromolecules* **1994**, *27*, 4639.

(51) Khokhlov, A. R.; Grosberg, A. Y.; Pande, V. S. *Statistical Physics of Macromolecules*; AIP Press: Jericho, NY, 1994.

(52) Flory, P. J. Spatial Configuration of Macromolecular Chains. *Science* **1975**, *188*, 1268.

(53) Wittmer, J. P.; Meyer, H.; Baschnagel, J.; Johner, A.; Obukhov, S.; Mattioni, L.; Müller, M.; Semenov, A. N. Long range bond-bond correlations in dense polymer solutions. *Phys. Rev. Lett.* **2004**, *93*, 147801.

(54) Wittmer, J. P.; Beckrich, P.; Meyer, H.; Cavallo, A.; Johner, A.; Baschnagel, J. Intramolecular long-range correlations in polymer melts: The segmental size distribution and its moments. *Phys. Rev. E* **2007**, *76*, 011803.

(55) Glaser, J.; Qin, J.; Medapuram, P.; Morse, D. C. Collective and single-chain correlations in disordered melts of symmetric diblock copolymers: Quantitative comparison of simulations and theory. *Macromolecules* **2014**, *47*, 851.

(56) Clark, A.; McCarty, J.; Guenza, M. Effective potentials for representing polymers in melts as chains of interacting soft particles. *J. Chem. Phys.* **2013**, *139*, 124906.

(57) McCarty, J.; Clark, A.; Copperman, J.; Guenza, M. An analytical coarse-graining method which preserves the free energy, structural correlations, and thermodynamic state of polymer melts from the atomistic to the mesoscale. *J. Chem. Phys.* **2014**, *140*, 204913.

(58) Freed, K. F. *Renormalization Group Theory of Macromolecules*; Wiley-Interscience: New York, 1987.

(59) Flory, P. J. The configuration of real polymer chains. *J. Chem. Phys.* **1949**, *17*, 303.

(60) Schmid, F. Self-consistent-field theories for complex fluids. *J. Phys.: Condens. Matter* **1998**, *10*, 8105.

(61) Müller, M.; Schmid, F. *Advanced Computer Simulation Approaches for Soft Matter Sciences II*; Springer: 2005; p 1.

(62) Fredrickson, G. H.; Helfand, E. Fluctuation effects in the theory of microphase separation in block copolymers. *J. Chem. Phys.* **1987**, *87*, 697.

(63) Witten, T. A.; Milner, S. T.; Wang, Z.-G. In *Multiphase Macromolecular Systems*; Culbertson, B., Ed.; Plenum Press: New York, 1989; p 655.

(64) Fetters, L. J.; Lohse, D. J.; Milner, S. T.; Graessley, W. W. Packing length influence in linear polymer melts on the entanglement, critical, and reptation molecular weights. *Macromolecules* **1999**, *32*, 6847.

(65) Müller, M. In *Hybrid Particle-Continuum Methods in Computational Materials Physics*; Müser, M. H., Sutmann, G., Winkler, R. G., Eds.; Forschungszentrum Jülich: 2013; Vol. *46*, p 127.

(66) Zhang, G.; Stuehn, T.; Daoulas, K. C.; Kremer, K. One size fits all: Equilibrating chemically different polymer liquids through universal long-wavelength description. *J. Chem. Phys.* **2015**, *142*, 221102.

(67) Edwards, S. F. Statistical mechanics with topological constraints: I. *Proc. Phys. Soc., London* **1967**, *91*, 513.

(68) Fetters, L. J.; Lohse, D. J.; Graessley, W. W. Chain dimensions and entanglement spacings in dense macromolecular systems. *J. Polym. Sci., Part B: Polym. Phys.* **1999**, *37*, 1023.

(69) Lin, Y.-H. Number of entanglement strands per cubed tube diameter, a fundamental aspect of topological universality in polymer viscoelasticity. *Macromolecules* **1987**, *20*, 3080.

(70) Kavassalis, T. A.; Noolandi, J. New view of entanglements in dense polymer systems. *Phys. Rev. Lett.* **1987**, *59*, 2674.

(71) Rosa, A.; Everaers, R. Ring polymers in the melt state: The physics of crumpling. *Phys. Rev. Lett.* **2014**, *112*, 118302.

(72) Everaers, R. Topological versus rheological entanglement length in primitive-path analysis protocols, tube models, and slip-link models. *Phys. Rev. E* **2012**, *86*, No. 022801.

(73) Uchida, N.; Grest, G. S.; Everaers, R. Viscoelasticity and primitive path analysis of entangled polymer liquids: From F-actin to polyethylene. *J. Chem. Phys.* **2008**, *128*, No. 044902.

(74) de Gennes, P. G. Reptation of a polymer chain in the presense of fixed obstacles. *J. Chem. Phys.* **1971**, *55*, 572.

(75) Edwards, S. F. The statistical mechanics of polymerized material. *Proc. Phys. Soc., London* **1967**, *92*, 9.

(76) Fetters, L. J.; Lohse, D. J.; Colby, R. H. In *Physical Properties of Polymers Handbook*; Mark, J., Ed.; Springer: 2007; p 447.

(77) Uchida, N.; Grest, G. S.; Everaers, R. Viscoelasticity and primitive path analysis of entangled polymer liquids: From F-actin to polyethylene. *J. Chem. Phys.* **2008**, *128*, No. 044902.

(78) Bennemann, C.; Paul, W.; Binder, K.; Dünweg, B. Molecular-dynamics simulations of the thermal glass transition in polymer melts: α-relaxation behavior. *Phys. Rev. E* **1998**, *57*, 843.

(79) Buchholz, J.; Paul, W.; Varnik, F.; Binder, K. Cooling rate dependence of the glass transition temperature of polymer melts: Molecular dynamics study. *J. Chem. Phys.* **2002**, *117*, 7364.

(80) Grest, G.; Communication, S. Polymer entanglement dynamics: Role of attractive interactions. *J. Chem. Phys.* **2016**, *145*, 141101.

(81) Meyer, H.; Müller-Plathe, F. Formation of chain-folded structures in supercooled polymer melts. *J. Chem. Phys.* **2001**, *115*, 7807−7810.

(82) Hoy, R. S.; Karayiannis, N. C. Simple model for chain packing and crystallization of soft colloidal polymers. *Phys. Rev. E* **2013**, *88*, No. 012601.

(83) Morthomas, J.; Fusco, C.; Zhai, Z.; Lame, O.; Perez, M. Crystallization of finite-extensible nonlinear elastic Lennard-Jones coarse-grained polymers. *Phys. Rev. E: Stat. Phys., Plasmas, Fluids, Relat. Interdiscip. Top.* **2017**, *96*, No. 052502.

(84) Meyer, S.; Jost, D.; Theodorakopoulos, N.; Peyrard, M.; Lavery, R.; Everaers, R. Temperature dependence of the DNA double helix at the nanoscale: Structure, elasticity, and fluctuations. *Biophys. J.* **2013**, *105*, 1904.

(85) Treloar, L. R. G. *The Physics of Rubber Elasticity*; Oxford University Press: 1975.

(86) Hsu, H.-P.; Kremer, K. A coarse-grained polymer model for studying the glass transition. *J. Chem. Phys.* **2019**, *150*, 091101.

(87) Gotro, J. T.; Graessley, W. W. Model hydrocarbon polymers: rheological properties of linear polyisoprenes and hydrogenated polyisoprenes. *Macromolecules* **1984**, *17*, 2767.

(88) Abdel-Goad, M.; Pyckhout-Hintzen, W.; Kahle, S.; Allgaier, J.; Richter, D.; Fetters, L. J. Rheological properties of 1, 4-polyisoprene over a large molecular weight range. *Macromolecules* **2004**, *37*, 8135.

(89) Vaca Chávez, F.; Saalwächter, K. Time-domain NMR observation of entangled polymer dynamics: Universal behavior of flexible homopolymers and applicability of the tube model. *Macromolecules* **2011**, *44*, 1549.

(90) Auhl, D.; Ramirez, J.; Likhtman, A. E.; Chambon, P.; Fernyhough, C. Linear and nonlinear shear flow behavior of monodisperse polyisoprene melts with a large range of molecular weights. *J. Rheol.* **2008**, *52*, 801.

(91) van Meerveld, J. A method to extract the monomer friction coefficient from the linear viscoelastic behavior of linear, entangled polymer melts. *Rheol. Acta* **2004**, *43*, 615.

(92) Niedzwiedz, K.; Wischnewski, A.; Pyckhout-Hintzen, W.; Allgaier, J.; Richter, D.; Faraone, A. Chain dynamics and viscoelastic properties of poly (ethylene oxide). *Macromolecules* **2008**, *41*, 4866.

(93) Richter, D.; Monkenbusch, M.; Arbe, A.; Colmenero, J. *Neutron Spin Echo in Polymer Systems*; Springer: 2005; p 1.

(94) Bird, R. B.; Armstrong, R. C.; Hassager, O. *Dynamics of Polymeric Liquids*; Wiley: New York, 1987; Vol. 1.

(95) Watanabe, H. Viscoelasticity and dynamics of entangled polymers. *Prog. Polym. Sci.* **1999**, *24*, 1253−1403.

(96) Saalwächter, K. Proton multiple-quantum NMR for the study of chain dynamics and structural constraints in polymeric soft materials. *Prog. Nucl. Magn. Reson. Spectrosc.* **2007**, *51*, 1.

(97) Arbe, A.; Monkenbusch, M.; Stellbrink, J.; Richter, D.; Farago, B.; Almdal, K.; Faust, R. Origin of internal viscosity effects in flexible polymers: A comparative neutron spin-echo and light scattering study on poly (dimethylsiloxane) and polyisobutylene. *Macromolecules* **2001**, *34*, 1281.

(98) Unidad, H. J.; Goad, M. A.; Bras, A. R.; Zamponi, M.; Faust, R.; Allgaier, J.; Pyckhout-Hintzen, W.; Wischnewski, A.; Richter, D.; Fetters, L. J. Consequences of increasing packing length on the dynamics of polymer melts. *Macromolecules* **2015**, *48*, 6638.

(99) Likhtman, A.; McLeish, T. Quantitative theory for linear dynamics of linear entangled polymers. *Macromolecules* **2002**, *35*, 6332.

(100) Hou, J.-X.; Svaneborg, C.; Everaers, R.; Grest, G. S. Stress relaxation in entangled polymer melts. *Phys. Rev. Lett.* **2010**, *105*, 068301.

(101) Faller, R. Coarse-grain modeling of polymers. *Rev. Comp. Ch.* **2007**, *23*, 233.

(102) Peter, C.; Kremer, K. Multiscale simulation of soft matter systems. *Faraday Discuss.* **2010**, *144*, 9.

(103) Hahn, O.; Site, L. D.; Kremer, K. Simulation of polymer melts: From spherical to ellipsoidal beads. *Macromol. Theory Simul.* **2001**, *10*, 288.

(104) Masubuchi, Y.; Uneyama, T. Comparison among multi-chain models for entangled polymer dynamics. *Soft Matter* **2018**, *14*, 5986.

(105) Takahashi, K. Z.; Nishimura, R.; Yamato, N.; Yasuoka, K.; Masubuchi, Y. Onset of static and dynamic universality among molecular models of polymers. *Sci. Rep.* **2017**, *7*, 12379.

(106) Halverson, J. D.; Lee, W. B.; Grest, G. S.; Grosberg, A. Y.; Kremer, K. Molecular Dynamics simulation study of nonconcatenated ring polymers in a melt. *J. Chem. Phys.* **2011**, *134*, 204904.

(107) Ianniruberto, G.; Brasiello, A.; Marrucci, G. Simulations of fast shear flows of PS oligomers confirm monomeric friction reduction in fast elongational flows of monodisperse PS melts as indicated by rheooptical data. *Macromolecules* **2012**, *45*, 8058.

(108) Yaoita, T.; Isaki, T.; Masubuchi, Y.; Watanabe, H.; Ianniruberto, G.; Marrucci, G. Primitive chain network simulation of elongational flows of entangled linear chains: stretch/orientation-induced reduction of monomeric friction. *Macromolecules* **2012**, *45*, 2773.

(109) Ciccotti, G.; Ferrario, M.; Ryckaert, J.-P. Molecular dynamics of rigid systems in cartesian coordinates: A general formulation. *Mol. Phys.* **1982**, *47*, 1253.

(110) Hua, C. C.; Schieber, J. D. Segment connectivity, chain-length breathing, segmental stretch, and constraint release in reptation models. I. Theory and single-step strain predictions. *J. Chem. Phys.* **1998**, *109*, 10018.

(111) Masubuchi, Y.; Takimoto, J.-I.; Koyama, K.; Ianniruberto, G.; Marrucci, G.; Greco, F. Brownian simulations of a network of reptating primitive chains. *J. Chem. Phys.* **2001**, *115*, 4387.

(112) Likhtman, A. E. Single-chain slip-link model of entangled polymers: Simultaneous description of neutron spin-echo, rheology, and diffusion. *Macromolecules* **2005**, *38*, 6128.

(113) Chappa, V. C.; Morse, D. C.; Zippelius, A.; Müller, M. Translationally invariant slip-spring model for entangled polymer dynamics. *Phys. Rev. Lett.* **2012**, *109*, 148302.

(114) Vogiatzis, G. G.; Megariotis, G.; Theodorou, D. N. Equation of state based slip spring model for entangled polymer dynamics. *Macromolecules* **2017**, *50*, 3004.

(115) Kremer, K. In *Soft and Fragile Matter: Non Equilibrium Dynamics, Metastability and Flow*; Cates, M. E., Evans, M. R., Eds.; J.W. Arrowsmith Ltd.: Bristol, UK, 2000; p 145.

(116) Kremer, K. Computer simulations for macromolecular science. *Macromol. Chem. Phys.* **2003**, *204*, 257.

(117) Marrink, S. J.; Risselada, H. J.; Yefimov, S.; Tieleman, D. P.; De Vries, A. H. The MARTINI force field: Coarse grained model for biomolecular simulations. *J. Phys. Chem. B* **2007**, *111*, 7812.

(118) Lyubartsev, A. P.; Laaksonen, A. Calculation of effective interaction potentials from radial distribution functions: A reverse Monte Carlo approach. *Phys. Rev. E* **1995**, *52*, 3730.

(119) Izvekov, S.; Voth, G. A. Multiscale coarse graining of liquid-state systems. *J. Chem. Phys.* **2005**, *123*, 134105.

(120) Rühle, V.; Junghans, C.; Lukyanov, A.; Kremer, K.; Andrienko, D. Versatile object-oriented toolkit for coarse-graining applications. *J. Chem. Theory Comput.* **2009**, *5*, 3211.

(121) Mori, H. Transport, collective motion, and Brownian motion. *Prog. Theor. Phys.* **1965**, *33*, 423.

(122) Nordholm, S.; Zwanzig, R. A systematic derivation of exact generalized Brownian motion theory. *J. Stat. Phys.* **1975**, *13*, 347.

(123) Hijón, C.; Español, P.; Vanden-Eijnden, E.; Delgado-Buscalioni, R. Mori−Zwanzig formalism as a practical computational tool. *Faraday Discuss.* **2010**, *144*, 301.

(124) Carof, A.; Vuilleumier, R.; Rotenberg, B. Two algorithms to compute projected correlation functions in molecular dynamics simulations. *J. Chem. Phys.* **2014**, *140*, 124103.

(125) Jung, G.; Hanke, M.; Schmid, F. Iterative reconstruction of memory kernels. *J. Chem. Theory Comput.* **2017**, *13*, 2481−2488.

(126) Soddemann, T.; Dünweg, B.; Kremer, K. Dissipative particle dynamics: A useful thermostat for equilibrium and nonequilibrium molecular dynamics simulations. *Phys. Rev. E* **2003**, *68*, No. 046702.

(127) Moreira, L. A.; Zhang, G.; Müller, F.; Stuehn, T.; Kremer, K. Direct equilibration and characterization of polymer melts for computer simulations. *Macromol. Theory Simul.* **2015**, *24*, 419.

(128) Svaneborg, C.; Karimi-Varzaneh, H. A.; Hojdis, N.; Fleck, F.; Everaers, R. Multiscale approach to equilibrating model polymer melts. *Phys. Rev. E* **2016**, *94*, No. 032502.

(129) Sirk, T. W.; Slizoberg, Y. R.; Brennan, J. K.; Lisal, M.; Andzelm, J. W. An enhanced entangled polymer model for dissipative particle dynamics. *J. Chem. Phys.* **2012**, *136*, 134903.

(130) Tries, V.; Paul, W.; Baschnagel, J.; Binder, K. Modeling polyethylene with the bond fluctuation model. *J. Chem. Phys.* **1997**, *106*, 738.

(131) Baiesi, M.; Barkema, G. T.; Carlon, E. Elastic lattice polymers. *Phys. Rev. E* **2010**, *81*, No. 061801.

(132) Schram, R.; Barkema, G. Simulation of ring polymer melts with GPU acceleration. *J. Comput. Phys.* **2018**, *363*, 128.

(133) Everaers, R.; Sukumaran, S. K.; Grest, G. S.; Svaneborg, C.; Sivasubramanian, A.; Kremer, K. Rheology and microscopic topology of entangled polymeric liquids. *Science* **2004**, *303*, 823.

(134) Carbone, P.; Karimi-Varzaneh, H. A.; Müller-Plathe, F. Fine-graining without coarse-graining: An easy and fast way to equilibrate dense polymer melts. *Faraday Discuss.* **2010**, *144*, 25.

(135) Graessley, W. W. Entangled linear, branched and network polymer systems — Molecular theories. *Adv. Polym. Sci.* **1982**, *47*, 67.

(136) Marrucci, G. Relaxation by reptation and tube enlargement: A model for polydisperse polymers. *J. Polym. Sci., Polym. Phys. Ed.* **1985**, *23*, 159.

(137) Rubinstein, M.; Colby, R. H. Self-consistent theory of polydisperse entangled polymers: Linear viscoelasticity of binary blends. *J. Chem. Phys.* **1988**, *89*, 5291.

(138) Marrucci, G.; Ianniruberto, G. Flow-induced orientation and stretching of entangled polymers. *Philos. Trans. R. Soc., A* **2003**, *361*, 677.

(139) Ianniruberto, G.; Marrucci, G. Convective constraint release (CCR) revisited. *J. Rheol.* **2014**, *58*, 89.

(140) Rosa, A.; Everaers, R. Structure and dynamics of interphase chromosomes. *PLoS Comput. Biol.* **2008**, *4*, e1000153.

(141) Halverson, J. D.; Grest, G. S.; Grosberg, A. Y.; Kremer, K. Rheology of ring polymer melts: From linear contaminants to ring-linear blends. *Phys. Rev. Lett.* **2012**, *108*, 038301.

(142) Grest, G. S.; Kremer, K.; Milner, S. T.; Witten, T. A. Relaxation of self-entangled many-arm star polymers. *Macromolecules* **1989**, *22*, 1904.

(143) Grest, G. S.; Kremer, K. Statistical properties of random cross-linked rubbers. *Macromolecules* **1990**, *23*, 4994.

(144) Duering, E. R.; Kremer, K.; Grest, G. S. Relaxation of randomly cross-linked polymer melts. *Phys. Rev. Lett.* **1991**, *67*, 3531.

(145) Svaneborg, C.; Grest, G. S.; Everaers, R. Strain-dependent localization, microscopic deformations, and macroscopic normal tensions in model polymer networks. *Phys. Rev. Lett.* **2004**, *93*, 257801.

(146) Svaneborg, C.; Everaers, R.; Grest, G. S.; Curro, J. G. Connectivity and entanglement stress contributions in strained polymer networks. *Macromolecules* **2008**, *41*, 4920.

(147) Aoyagi, T.; Takimoto, J.-I.; Doi, M. Molecular Dynamics study of polymer melt confined between walls. *J. Chem. Phys.* **2001**, *115*, 552.

(148) Pierce, F.; Perahia, D.; Grest, G. S. Interdiffusion of short chain oligomers into an entangled polymer film. *Macromolecules* **2009**, *42*, 7969.

(149) Murat, M.; Grest, G. S. Polymers end-grafted onto a cylindrical surface. *Macromolecules* **1991**, *24*, 704.

(150) Murat, M.; Grest, G. S. Interaction between grafted polymeric brushes: A Molecular Dynamics study. *Phys. Rev. Lett.* **1989**, *63*, 1074.

(151) Grest, G. S. Interfacial sliding of polymer brushes: a Molecular Dynamics simulation. *Phys. Rev. Lett.* **1996**, *76*, 4979.

(152) Yagyu, H.; Utsumi, T. Coarse-grained Molecular Dynamics simulation of nanofilled crosslinked rubber. *Comput. Mater. Sci.* **2009**, *46*, 286.

(153) Sussman, D. M.; Tung, W.-S.; Winey, K. I.; Schweizer, K. S.; Riggleman, R. A. Entanglement reduction and anisotropic chain and primitive path conformations in polymer melts under thin film and cylindrical confinement. *Macromolecules* **2014**, *47*, 6462.

(154) Gersappe, D. Molecular mechanisms of failure in polymer nanocomposites. *Phys. Rev. Lett.* **2002**, *89*, 058301.

(155) Ge, T.; Robbins, M. O.; Perahia, D.; Grest, G. S. Healing of polymer interfaces: Interfacial dynamics, entanglements, and strength. *Phys. Rev. E* **2014**, *90*, 012602.

(156) Zhang, W.; Gomez, E. D.; Milner, S. T. Predicting Flory-Huggins χ from Simulations. *Phys. Rev. Lett.* **2017**, *119*, No. 017801.

(157) Bennemann, C.; Baschnagel, J.; Paul, W.; Binder, K. Molecular-dynamics simulation of a glassy polymer melt: Rouse model and cage effect. *Comput. Theor. Polym. Sci.* **1999**, *9*, 217.

(158) Baschnagel, J.; Varnik, F. Computer simulations of super-cooled polymer melts in the bulk and in confined geometry. *J. Phys.: Condens. Matter* **2005**, *17*, R851.

(159) Williams, M. L.; Landel, R. F.; Ferry, J. D. The temperature dependence of relaxation mechanisms in amorphous polymers and other glass-forming liquids. *J. Am. Chem. Soc.* **1955**, *77*, 3701.

(160) Vogel, H. The law of the relation between the viscosity of liquids and the temperature. *Phys. Z.* **1921**, *22*, 654.

(161) Fulcher, G. S. Analysis of recent measurements of the viscosity of glasses. *J. Am. Ceram. Soc.* **1925**, *8*, 339.

(162) Tammann, G.; Hesse, W. The dependence of viscosity upon the temperature of supercooled liquids. *Z. Anorg. Allg. Chem.* **1926**, *156*, 245.

(163) Plimpton, S. Fast parallel algorithms for short-range Molecular Dynamics. *J. Comput. Phys.* **1995**, *117*, 1.